

Identification of a natural fieldlike entanglement resource in trapped-ion chains

Natalie Klco^{1,*} and D. H. Beck^{2,†}

¹*Duke Quantum Center and Department of Physics, Duke University, Durham, North Carolina 27708, USA*

²*Department of Physics and Illinois Quantum Information Science and Technology Center, University of Illinois at Urbana-Champaign, Urbana, Illinois 61801, USA*



(Received 6 December 2023; revised 6 May 2024; accepted 8 May 2024; published 13 June 2024)

The electromagnetic trapping of ion chains can be regarded as a process of nontrivial entangled quantum state preparation within Hilbert spaces of the local axial motional modes. To begin uncovering properties of this entanglement resource produced as a by-product of conventional ion-trap quantum information processing, the quantum continuous-variable formalism is herein utilized to focus on the leading-order entangled ground state of local motional modes in the presence of a quadratic trapping potential. The decay of entanglement between disjoint subsets of local modes is found to exhibit features of entanglement structure and responses to partial measurement reminiscent of the free massless scalar field vacuum. With significant fidelities between the two, even for large system sizes, a framework is established for initializing quantum field simulations by “imaging” extended entangled states from natural sources, rather than building correlations through deep circuits of few-body entangling operators. By calculating probabilities in discrete Fock subspaces of the local motional modes, we present considerations for locally transferring these pre-distributed entanglement resources to the qudits of ion internal energy levels, improving this procedure’s anticipated experimental viability.

DOI: [10.1103/PhysRevA.109.062419](https://doi.org/10.1103/PhysRevA.109.062419)

I. INTRODUCTION

Spatially distributed quantum correlations not only play an important role in the structure, observed dynamics, and apparent thermalization of quantum many-body systems [1–19] but also act as a fundamental resource in designing and operating quantum computation, simulation, sensing, and communication technologies [20–31]. For such applications, the necessary entanglement is commonly produced via a series of direct interactions generated between two or more quantum degrees of freedom or distributed after production through quantum networking techniques that maintain coherence throughout transmission. A third possibility, however, relies upon connecting locally to a shared system of naturally distributed entanglement (see Fig. 1). For example, the vacuum state of a quantum field is entangled at spacelike separations [32–36], and a pair of locally interacting detectors can transfer that entanglement into basic quantum degrees of freedom [37–39] to drive subsequent quantum information-processing protocols. While the raw entanglement produced through this type of extraction is expected to be far smaller than what can be generated through artificially constructed logic gates, “imaging” natural entanglement can provide a valuable structure of quantum correlations, e.g., as a starting point for large-scale quantum simulations of physical systems or the generation of entangled sensing arrays. The present paper focuses on the local axial motional modes of a trapped-ion chain, quantifying their entanglement properties and utilizing

this information to guide applications in the quantum simulation of quantum fields.

With each global motional mode in its ground state, the vacuum of ion-chain zero-point fluctuations is an unentangled, tensor-product state with respect to partitions among the normal modes. However, for partitions among the associated local motional modes, this vacuum exhibits entanglement and, to a good approximation for practical trapping potentials, constitutes a Gaussian continuous-variable (CV) system. Note that the ion chain supports both transverse and axial modes (see Ref. [40] for a recent review). While the global motional modes are commonly utilized to mediate all-to-all entangling gates among ions within the trap [41–46], the local transverse motional modes have been proposed to represent computational bosonic degrees of freedom in the design of lattice-gauge-theory quantum simulations [47,48].

For a pair of disjoint regions within the global vacuum state, each comprising the fluctuations associated with one or more consecutive ions, it is herein found that many entanglement characteristics are remarkably similar to those of the massless noninteracting lattice scalar field vacuum. In particular, the logarithmic negativity between the regions decreases exponentially with increasing separation, whereas the corresponding two-point functions decrease, at most, as a power law. As with the scalar field vacuum, the stronger entanglement represented by the two-point functions can also be recovered with classical communication of measurements on parts of the system external to the two regions [49].

After the local axial modes of the trapped-ion vacuum are presented as a Gaussian CV system in Sec. II, its entanglement characteristics are described with reference to those of the scalar field vacuum in Sec. III. Two possible applications

*natalie.klco@duke.edu

†dhbeck@illinois.edu

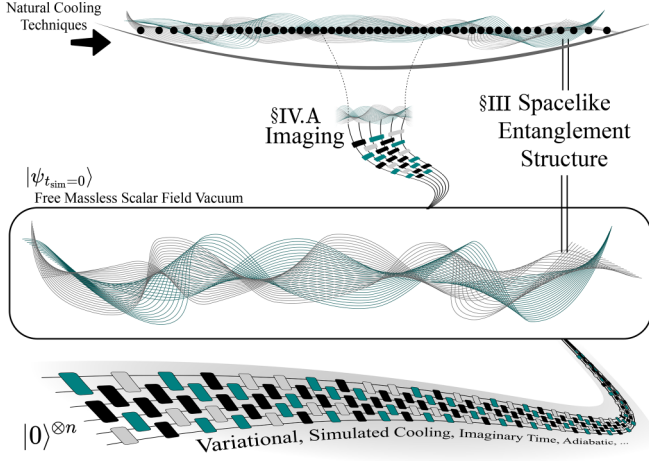


FIG. 1. As discussed in Sec. III, the structure of spacelike distributed entanglement between disjoint regions of the free massless scalar field vacuum is similar to that of the axial modes in a trapped-ion-chain motional ground state. Motivated by this observation, We propose cooled motional modes in Sec. IV as an entanglement resource that may be imaged as an alternative method of vacuum-state preparation for scattering and quantum field simulations.

are subsequently discussed in Sec. IV using the trapped-ion vacuum both as a state preparation resource for the scalar field vacuum and as a more general resource from which entanglement can be transferred into the discrete-variable framework of ion internal states.¹

In our pursuit of these applications, the entanglement structure provided essential guidance, e.g., by indicating that the scalar field vacuum and axial modes of the ion-chain motional ground state naturally contain similar distributions of quantum correlations or by identifying the dominant collective modes to optimize entanglement transfer. While the connections explored here represent only early observations, this concrete example suggests significant opportunities for incorporating natural sources of distributed entanglement as active components in quantum technologies.

II. LOCAL AXIAL MOTIONAL MODES

The Hamiltonian describing N ions in a one-dimensional linear trap is the sum of the ion kinetic energies T and Coulomb interactions within the trapping potential U ,

$$T = \sum_{i=1}^N \frac{m\dot{z}_i^2}{2}, \quad (1)$$

$$U = \sum_{i=1}^N q\kappa_2 z_i^2 + \frac{1}{2} \sum_{\substack{i,j=1 \\ i \neq j}}^N \frac{q^2}{4\pi\epsilon_0 |z_i - z_j|}, \quad (2)$$

where q and m are the charge and mass of each ion (assuming homogeneous ion species), κ_2 is the strength of the quadratic trapping potential, and z_i is the position of the i th ion along the

one-dimensional trap axis [50,51]. Although the incorporation of anharmonicities in the trapping potential [52,53] will be of future interest, e.g., for opportunities to design ion spacings that produce local motional modes with a regularity that mirrors conventional latticizations of field theories, the current work utilizes a quadratic trapping potential.

As usual, the equilibrium positions of ions within the trap may be calculated by solving the set of equations enforcing vanishing first derivatives of the potential with respect to displacements,

$$\left. \frac{\partial U}{\partial z_i} \right|_{z=z_0} = \vec{0}, \quad (3)$$

to place each ion in a stable local minimum. For small systems, these equations can be solved exactly (see Appendix A). For larger systems, the equilibrium positions can be reliably calculated numerically [54,55]. The central ions of these large chains develop an approximately evenly spaced distribution, with the edges systematically relaxing to larger separations as the soft harmonic potential is countered by the center-dominated Coulomb repulsion.

The above Hamiltonian has two significant scales, one associated with the interior spacing and one associated with oscillations of the ions about their equilibrium positions. Isolating these characteristic scales to identify a dimensionless description of the system, the Hamiltonian may be written as

$$H = \frac{m\omega_z^2 \ell_{\mu m}^2}{2} \sum_{i=1}^N \left(\dot{\bar{z}}_i^2 + \bar{z}_i^2 + \sum_{\substack{j=1 \\ j \neq i}}^N \frac{1}{|\bar{z}_i - \bar{z}_j|} \right) \quad (4)$$

$$= \frac{m\omega_z^2 \ell_{\mu m}^2}{2} (\bar{T} + \bar{U}), \quad (5)$$

where $\bar{z} = \frac{z}{\ell_{\mu m}}$ and $\dot{\bar{z}} = \frac{\dot{z}}{\omega_z \ell_{\mu m}}$. The characteristic spacing and oscillation parameters are $\ell_{\mu m} = \left(\frac{q}{8\pi\epsilon_0\kappa_2}\right)^{\frac{1}{3}}$ and $\omega_z^2 = \frac{2q\kappa_2}{m}$, where the latter is the center-of-mass oscillation frequency for an ion chain. The root-mean-square of fluctuations from equilibrium in the ground state of an oscillator of this frequency yields the length $\ell_{nm} = \sqrt{\frac{\hbar}{m\omega_z}}$. To provide a sense of scale for these two lengths, a single $^{171}\text{Yb}^+$ ion in a trap with $\omega_z/2\pi = 1\text{MHz}$ yields fluctuations characterized by the scale $\ell_{nm} = 7.7\text{ nm}$, while the separation between such ions is governed by the larger scale $\ell_{\mu m} = 2.7\mu\text{m}$. As such, the lengths have been labeled for their canonical magnitudes in a broad regime of trapped-ion applications.

With a second set of variables defined and scaled for excursions from equilibrium positions, $\bar{\xi} = \frac{z-z_0}{\ell_{nm}} = (\bar{z} - \bar{z}_0) \frac{\ell_{\mu m}}{\ell_{nm}}$, the potential may be expanded about the equilibrium as

$$U = \frac{\hbar\omega_z}{2} \frac{\ell_{\mu m}^2}{\ell_{nm}^2} \left(\frac{1}{2!} \left. \frac{\partial^2 \bar{U}}{\partial \bar{z}_i \partial \bar{z}_j} \right|_{\bar{z}=\bar{z}_0} \left(\frac{\ell_{nm}}{\ell_{\mu m}} \right)^2 \bar{\xi}_i \bar{\xi}_j + \frac{1}{3!} \left. \frac{\partial^3 \bar{U}}{\partial \bar{z}_i \partial \bar{z}_j \partial \bar{z}_k} \right|_{\bar{z}=\bar{z}_0} \left(\frac{\ell_{nm}}{\ell_{\mu m}} \right)^3 \bar{\xi}_i \bar{\xi}_j \bar{\xi}_k + \dots \right), \quad (6)$$

where a shift has been introduced to place the equilibrium configuration at zero potential, $\bar{U}(\bar{z}_0) = 0$. With higher-order contributions suppressed by powers of $\frac{\ell_{nm}}{\ell_{\mu m}}$, the convergence

¹Note that the scalar field is also referred to as a harmonic chain or Klein-Gordon field.

of this expansion is commonly rapid. For the representative $^{171}\text{Yb}^+$ example considered above, this ratio is 2.8×10^{-3} . Implementing a harmonic approximation of the potential, the leading-order dimensionless Hamiltonian describing small oscillations about equilibrium is

$$\bar{H}_2 = \sum_{i=1}^N \hat{\zeta}_i^2 + \sum_{i,j=1}^N \bar{\zeta}_i \bar{L}_{ij} \bar{\zeta}_j, \quad (7)$$

where $H_2 = \frac{\hbar\omega_z}{2} \bar{H}_2$ and $\bar{L}_{ij} = \frac{1}{2} \frac{\partial^2 \bar{U}}{\partial \bar{z}_i \partial \bar{z}_j} |_{\bar{z}=\bar{z}_0}$ is the Hessian matrix of second derivatives. In the following, this harmonicity supports the use of the Gaussian continuous-variable formalism [56,57], allowing the leading-order entanglement information of the ground state to be succinctly captured by the covariance matrix alone.

By diagonalizing the potential, axial normal modes of motion may be calculated as position-space eigenvectors \mathbf{e}_α of the Hessian with eigenvalues $\bar{\omega}_\alpha^2$ in units of the center-of-mass oscillation frequency, $\bar{\omega} = \omega/\omega_z$. In this basis of normal modes, the dimensionless Hamiltonian operator is that of a set of independent oscillators,

$$\hat{H}_2 = \sum_{\alpha} \hat{v}_{\alpha}^2 + \bar{\omega}_{\alpha}^2 \hat{\xi}_{\alpha}^2, \quad (8)$$

with $\hat{\xi}_{\alpha}$ and \hat{v}_{α} being the dimensionless position and momentum operators, respectively, of the chain's normal modes. As usual, these operators may be written in terms of normal-mode creation and annihilation operators,

$$\hat{\xi}_{\alpha} = \frac{\hat{\xi}_{\alpha}}{\ell_{nm}} = \frac{\hat{a}_{\alpha} + \hat{a}_{\alpha}^{\dagger}}{\sqrt{2\bar{\omega}_{\alpha}}}, \quad (9)$$

$$\hat{v}_{\alpha} = \frac{\ell_{nm}}{\hbar} \hat{v}_{\alpha} = -i\sqrt{\frac{\bar{\omega}_{\alpha}}{2}} (\hat{a}_{\alpha} - \hat{a}_{\alpha}^{\dagger}), \quad (10)$$

with $[\hat{a}_{\alpha}, \hat{a}_{\beta}^{\dagger}] = \delta_{\alpha\beta}$. Naturally, the matrix of normal-mode eigenvectors \mathbf{e} , constructed in rows as $e_{\alpha,i} = (e_{\alpha})_i$, provides the unitary basis transformation between global and local motional modes:

$$\hat{\phi} = \mathbf{e}^{-1} \hat{\xi}, \quad \hat{\pi} = \mathbf{e}^{-1} \hat{v}, \quad (11)$$

where $\hat{\phi}$ and $\hat{\pi}$ are the vectors of position and conjugate-momentum operators for the local motional modes, respectively. A visualization of the ion chain and trap geometry is provided in Fig. 2, showing the global normal modes and their linear combinations that produce the basis of local axial motional modes.

In the global normal-mode vacuum, $\hat{a}_{\alpha}|0\rangle = 0$, with two-point expectation values of $\bar{\omega}_{\alpha} \langle 0 | \hat{\xi}_{\alpha} \hat{\xi}_{\beta} | 0 \rangle = \frac{1}{\bar{\omega}_{\alpha}} \langle 0 | \hat{v}_{\alpha} \hat{v}_{\beta} | 0 \rangle = \frac{\delta_{\alpha\beta}}{2}$, the two-point functions of the local oscillators are

$$\frac{\langle 0 | \hat{\phi}_i \hat{\phi}_j | 0 \rangle}{\ell_{nm}^2} = \frac{1}{2} \sum_{\alpha=1}^N \frac{(\mathbf{e}^{-1})_{i\alpha} (\mathbf{e}^{-1})_{j\alpha}}{\bar{\omega}_{\alpha}}, \quad (12)$$

$$\frac{\ell_{nm}^2}{\hbar^2} \langle 0 | \hat{\pi}_i \hat{\pi}_j | 0 \rangle = \frac{1}{2} \sum_{\alpha=1}^N (\mathbf{e}^{-1})_{i\alpha} (\mathbf{e}^{-1})_{j\alpha} \bar{\omega}_{\alpha}. \quad (13)$$

In the local phase-space basis of $\hat{\mathbf{r}} = \{\hat{\phi}_1, \hat{\pi}_1, \hat{\phi}_2, \hat{\pi}_2, \dots, \hat{\phi}_N, \hat{\pi}_N\}$, where the commutation relations are encapsulated in the symplectic matrix $\Omega = -i[\hat{\mathbf{r}}, \hat{\mathbf{r}}^T] = \bigoplus_{j=1}^N iY$, with Y

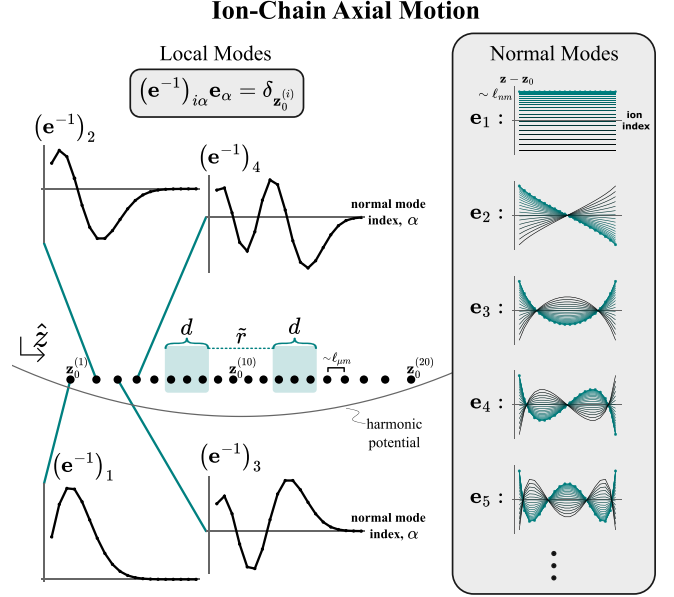


FIG. 2. For ions in a linear trap (center) with equilibrium positions $z_0^{(i)}$, normal modes of axial motion \mathbf{e}_α (right) may be linearly combined to form an alternate basis (left) describing the local motion of individual ions. The center diagram shows an example configuration of symmetrically distributed regions of size $d = 3$ and separation $\bar{r} = 4$ in a chain of $N = 20$ ions. Analogous to the tensor-product (entangled) structure of momentum (position) space partitions of the free scalar field vacuum, in the normal-mode ground state of ion motion, $\hat{a}_{\alpha}|0\rangle^{\otimes N} = 0$, partitions among the local modes are naturally entangled.

being the second Pauli matrix, the dimensionless ground-state covariance matrix (CM) is

$$\bar{\sigma}_{i,j} = \langle 0 | \{\hat{r}_i - \langle \hat{r}_i \rangle, \hat{r}_j - \langle \hat{r}_j \rangle\}_+ | 0 \rangle. \quad (14)$$

Examples of these covariance matrices for the local axial motional modes in small ion chains are provided in Appendix A. Because the vacuum expectation values of position-momentum anticommutators vanish,

$$\langle 0 | \{\hat{\phi}_i, \hat{\pi}_j\}_+ | 0 \rangle = 0, \quad (15)$$

the two point functions in Eqs. (12) and (13) fully determine the CM and thus the entanglement properties of the local motional modes in the leading-order Gaussian ground state.

The independence of the dimensionless CM, Eqs. (12)–(14), with respect to both trap and ion experimental parameters indicates a universality of the harmonic approximation [Eq. (6)] of the trapped-ion local motional mode correlation structure. With a single dimensionless CM to describe all ion choices and quadratic trap strengths, this universality results in leading-order insensitivity to experimental implementations. This may prove useful for error robustness or, conversely, may yield challenges because all modifications to the CM, e.g., for optimizing connections to the scalar field vacuum as discussed in Sec. IV A, must be implemented through explicit quantum operations. Furthermore, in this context, the dimensionful CM incorporates all ion and trap parameters through the length scale $\ell_{nm}^2 = \frac{\hbar}{\sqrt{2mq\kappa_2}}$,

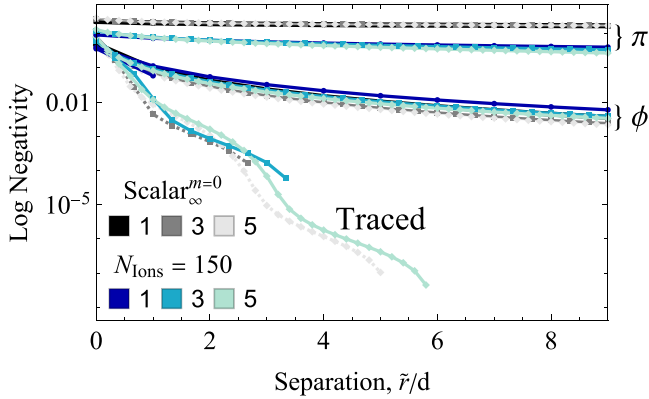


FIG. 3. Logarithmic negativity between two regions (of sizes $d = 1, 3, 5$ modes each) as a function of their separation in one spatial dimension. In the ion application (solid lines), each mode is a local axial motional mode, with the pair of regions centered within a 150-ion chain. In the scalar field application (dashed lines), each mode is a field lattice site within an infinite volume in the massless regime ($m = 10^{-10}$). Each system is shown when the volume external to the regions is traced or measured in the local position (ϕ) or local conjugate-momentum (π) basis.

which functions numerically as a global set of single-mode squeezing parameters with zero entanglement power, i.e., scaling the $\langle \hat{\phi}\hat{\phi} \rangle$ expectation values inversely from those of conjugate-momentum operators $\langle \hat{\pi}\hat{\pi} \rangle$ [see Eqs. (12) and (13)]. As such, leading-order entanglement quantities among local modes with a quadratic trapping potential are pure numbers independent of the variables of experimental design.

III. ENTANGLEMENT RESOURCE

To assess the entanglement naturally distributed among the local motional modes, consider entanglement properties between two disjoint regions, A and B , each composed of d contiguous ions and separated by \tilde{r} ions, as shown in the center of Fig. 2, for example. For this bipartite state, three logarithmic negativity values are of current interest: that when the local modes outside the regions are traced, resulting in an A - B mixed state, and those when the local modes outside the regions are projectively measured in the ϕ or π basis, resulting in A - B pure states.² With differing levels of classical information provided from possible external observers, these measures quantify here the operational amount of entanglement that could be consolidated into two-mode pairs spanning the disjoint regions [58–60].

As demonstrated in Fig. 3 for disjoint regions of local motional modes separated across the center of a 150-ion chain, the logarithmic negativity decays exponentially with the separation between regions upon tracing of the modes in the remaining chain [61–63]. Originating from a system with field (conjugate-momentum) two-point functions decaying logarithmically (polynomially) with spatial separation, the emergence of this strong decay is a result of the classical noise

introduced in the tracing procedure [49], i.e., resulting from the loss of information about an entangled quantum system. These features are common to the massless scalar field vacuum, for which Fig. 3 shows the analogous calculation in gray scale for reference. Beyond the magnitude and decay, the calculation in Fig. 3 also indicates close agreement in the separation at which the classical noise causes these regions of finite pixelation to transition into a regime of vanishing negativity [61–74] that is also separable [63,75]. With no free parameters, the externally traced logarithmic negativity is remarkably similar between these two distinct physical systems, one at the center of a quadratically trapped-ion chain and the other within an infinite volume of a free massless scalar field vacuum.

With the measurement of the external modes in the local position ϕ basis, Fig. 3 shows that the two systems again exhibit comparable underlying entanglement resources. However, with the measurement of the external modes in the conjugate-momentum π basis, the distinction between these two physical systems becomes apparent.³ This difference can be understood as a result of the field gradients in the scalar field and the quadratically balanced Coulomb repulsion in the trapped-ion chain distributing inequivalent vacuum entanglement.

Beyond the magnitudes of these entanglement measures, the local motional modes are found to have further structural entanglement features in common with the free lattice scalar field. Although the spatial parity symmetry, present when regions are centered within the ion chain, is generally insufficient for the techniques in Ref. [60] to ensure consolidation of negativity into a separable set of two-mode entangled pairs governed by partially transposed (PT) symplectic eigenvalues, it is found that the local motional modes within the trapped-ion chain do share this consolidation feature with the free scalar field vacuum. As such, the PT symplectic eigenvectors provide guidance for locally transforming the accessible many-body entanglement between disjoint regions of ions into a series of two-mode squeezed states. The availability of this two-mode organization of many-body mixed-state entanglement may prove to be useful experimentally in transferring entanglement from the local motional modes into discrete ion internal energy levels, as first proposed in Ref. [76] and further discussed in Sec. IV B.

IV. PRELIMINARY APPLICATIONS

A. Vacuum-state preparation

For digital quantum algorithms, studies establishing the efficiency (in, e.g., particle number, coupling strength, etc.) of simulating scattering in interacting quantum fields [77,78] show that the dominant use of quantum computational resources is expected to be required not in the real-time dynamics, but in the process of initial-state preparation, e.g., of the quantum field vacuum. From a complementary perspective, exploring the low-energy subspace and preparing states within it from a trivial tensor-product fiducial state can be

²See Ref. [49] for further technical details.

³Explicit forms of the classical noise removed upon measurement in each basis are provided in Ref. [49].

beyond the expected asymptotic efficiency of quantum hardware and software, even for few-body spatially local Hamiltonians [79–82]. These considerations, as well as the presence of phase transitions in lattice gauge theories, motivate the exploration of diverse methods of entangled quantum field vacuum-state preparation [73,83–98], with strategies ranging from variational techniques and guidance by tensor networks to adiabatic flows and the design of reservoirs for dynamical cooling procedures. To this vacuum-state-preparation literature, the present paper introduces the possibility of replacing the trivial-complexity fiducial state with an experimentally available state of naturally distributed entanglement.

When entanglement is generated through interleaved layers of few-body operators, entanglement is created with an expansion rate governed by the Lieb-Robinson bound [99,100]. However, when many-body entanglement resources are naturally present in a quantum architecture, e.g., the local motional modes of a trapped-ion chain, actively incorporating them in the algorithmic design can yield alternatives to propagation-based entanglement distribution. Analogous to the way in which providing a computational framework with quantum degrees of freedom allows more efficient representation and imitation of quantum systems themselves [20], providing a computational framework with access to naturally distributed arrays of entangled degrees of freedom could provide similar advantages for quantum field simulations.

For scalar field applications suggested by the entanglement observations above, consider quantifying the provided leading-order approximation with the quantum fidelity [22,101–103], $\mathcal{F}(\rho_1, \rho_2) = \mathcal{F}(\rho_2, \rho_1) = \text{tr}(\sqrt{\sqrt{\rho_1}\rho_2\sqrt{\rho_1}})$, where $\rho_{1,2}$ are the density matrices of local axial motional modes in the center of an ion chain and of CV lattice sites within an infinite-volume scalar field. The fidelity saturates to unity when the two density matrices are equivalent, vanishes when they are composed of orthogonal subspaces, and may be directly related to metrics providing a formal sense of distance between quantum states [104,105]. Furthermore, many preparation algorithms rely upon the availability of an input initial state with nonvanishing fidelity with respect to a desired state, impacting both figures of merit and necessary statistics.

For mixed Gaussian CV states, Ref. [106] provides several techniques for calculating the fidelity from the set of first and second moments of each Gaussian state.⁴ A fidelity analysis is shown in Fig. 4 between the local modes of the

⁴For example, when the first moments of both states are vanishing, the formulation [106]

$$\mathcal{F}(\sigma_1, \sigma_2) = \left(\frac{\det(2[\mathbb{I} + \frac{(V\Omega)^{-2}}{4} + \mathbb{I}]V)}{\det(\sigma_1 + \sigma_2)} \right)^{\frac{1}{4}}, \quad (16)$$

with

$$V = \Omega^T(\sigma_1 + \sigma_2)^{-1} \left(\frac{\Omega}{4} + \sigma_2\Omega\sigma_1 \right), \quad (17)$$

is straightforward to compute from the covariance matrices in the present harmonic approximation of the combined ion trapping and Coulomb potentials.

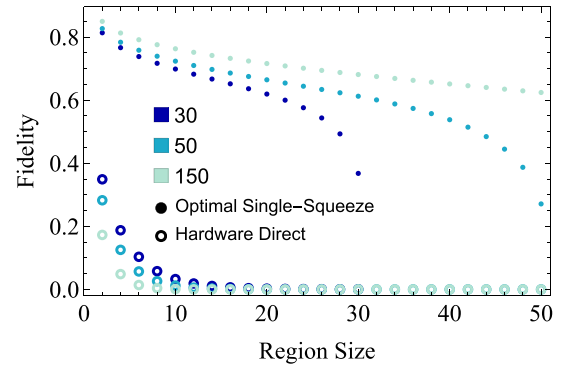


FIG. 4. Fidelity between the central local axial modes of trapped-ion chains cooled to their motional ground state and a same-size region of the infinite-volume, lattice scalar field vacuum in the massless regime ($m = 10^{-10}$). Shown for regions of up to 50 local modes/lattice sites for 30-, 50-, and 150-ion chains, a one-parameter optimization over a globally implemented single-mode squeezing parameter allows the creation of approximations to the latticized field vacuum with enduring fidelity.

trapped-ion motional ground state and the free, massless, lattice scalar field vacuum. Unfortunately, approximate quantum state preparations commonly yield fidelities that decay exponentially with increasing system size, becoming rapidly impractical for large-scale applications. As shown by the open points in Fig. 4, such catastrophic loss of fidelity occurs for the ion local motional modes naturally produced in the hardware. However, inspired by the similar distribution of disjoint two-region entanglement in both systems demonstrated in Fig. 3, we perform a one-parameter optimization of a single-mode squeezing applied to each local motional mode (a unitary with zero entanglement power), which results in substantial fidelities even for large systems. The values of this squeezing parameter as a function of region and chain size are recorded in the numerical tables in Appendix C. For chain lengths comparable to the field-region size, these squeezing magnitudes are realistic given current capabilities and ongoing developments in the experimental squeezing of ion motional modes [107–114]. Note that the universality of the dimensionless CM [Eqs. (12)–(14)] indicates that this squeezing must be introduced through external quantum operations on each local motional mode.

It is encouraging that a simply calculated set of local squeezings can produce a state of local motional modes with similar disjoint entanglement structure and $O(1)$ fidelity with respect to large instances of the massless lattice scalar field vacuum. The remaining fundamental distinctions between the small oscillation approximation of ion local motional modes and the scalar vacuum suggest that the calculated fidelity will not asymptote to unity for larger ion chains. However, note that this calculation considered only the flexibility of one single-mode squeezing parameter; for a given system, all entanglement features are thus generated only by the natural ion local motional modes themselves. As such, this calculation is best interpreted as a leading-order result, subject to systematic improvement upon the action of a broader array of CV quantum circuitry.

These preliminary results motivate dedicated future inquiry exploring the replacement of canonical tensor-product initial

states by experimentally convenient states of naturally distributed entanglement.

B. Transferring distributed entanglement

For the purposes of simulation with finite-dimensional quantum systems or for broader computational applications of spatially distributed quantum correlations, it is of interest to consider transferring the entanglement among local CV motional modes into the Hilbert space composed of the associated ions' internal energy levels. This process was first proposed as an opportunity for experimentally detecting vacuum entanglement and for entangling trapped ions with quantum gates utilizing only local phase-space excitations [76]. The local motional modes then provide an entangled fabric of spatially distributed entanglement that may be strategically accessed. That the naturally available entanglement structure is remarkably similar to that of a simple latticized quantum field suggests further possible applications from quantum simulation of standard-model physics to large-scale quantum error correction. Motivated by recent theoretical and experimental advances in qudit-based quantum information processing [115–127], the following section details one important consideration affecting the magnitude and efficiency of CV-to-qudit entanglement transfer in the context of trapped ions.

There are many strategies for transferring entanglement from CV local motional modes to finite-dimensional qudit systems [76,128–132]. One basic paradigm involves writing the CV system in an indexed orthonormal basis and performing an approximate swapping operation between n basis states and the n -dimensional qudit system. For example, Ref. [76] presents an approximation of such a SWAP operator for an expression of the CV local motional modes in the Fock basis, transferring the quantum information present in the low-energy Fock space to qubits of ion internal energy levels. Generalizing to qudits, the population of the CV system in states external to the chosen subspace (e.g., above the lowest-energy Fock states) yields excess population in the qudit initial state, reducing the transferred entanglement. For the Fock-space transfer, this external-population figure of merit is shown in Fig. 5 in Appendix B for the local motional modes of a two-ion chain as a function of increasing qudit dimension.

Although the entanglement between two Hilbert spaces is not impacted by local operations, the entanglement accessible from within a Hilbert space subset can be highly sensitive to local restructuring. As such, local CV operations applied prior to qudit extraction into the ion internal states can impact the probability in the qudit subspace and thus the transferred entanglement. Figure 5 indicates that first including a pair of single-mode squeezings to transform the local motional mode CM into normal form with balanced $\langle\phi\phi\rangle$ and $\langle\pi\pi\rangle$ matrix elements reduces the population external to the low-energy Fock states by several orders of magnitude, with the impact increasing with increasing qudit dimension. By directly calculating the motional mode CM naturally produced in the ion chain, such operations can be designed to optimize the localization of the ion modes in an experimentally convenient orthonormal basis for entanglement transfer.

In designing local operators for more than two ions to optimize this form of CV to finite-dimensional entanglement transfer, the observation discussed at the end of Sec. III—

that the ion local motional modes in this context satisfy requirements allowing the techniques in Ref. [60] to reorganize the available entanglement between regions—provides an additional advantage. Such consolidation, informed by the eigensystem of the partially transposed $2d$ -ion mixed state, reorganizes the bipartite entanglement between disjoint many-body field or ion-chain regions into a tensor-product series of $(1_A \times 1_B)$ entangled pairs. As such, this reorganization preconditions the CV entanglement to be conducive to subsequent entanglement transfer, ultimately allowing this entanglement to be consolidated into fewer ion pairs and improving the entanglement yield.

V. SUMMARY AND OUTLOOK

Considering entanglement structure from multiple operational perspectives can serve to quantify resources available for quantum information protocols and to guide the design of quantum simulations. This paper considered whether the local axial motional modes of a simple trapped-ion system can serve as a useful starting point for generation of entangled vacuum states of the massless scalar field. Because several region-region entanglement measures exhibit strong similarities between the two systems, analyses of fidelities and localization in Fock-space constitute initial steps toward utilizing naturally distributed entanglement resources for computational applications. This perspective highlights common elements among quantum simulation, sensing, and networking as quantum fields are considered for incorporation directly into quantum architectures.

The present analysis, however, only modestly addressed a subset of the important questions driving research toward quantum technology goals. For scientific application to quantum state preparation, the approximate correspondence observed in Sec. IV A must be promoted to a systematically improvable protocol, possibly through the introduction of a hierarchy of higher-complexity quantum operations [73,90]. Furthermore, future development toward quantum simulation applications should be made beyond the idealized motional vacuum to include experimentally attainable quantum states after cooling procedures minimize, but do not eliminate, collective phonon numbers.

For the application in Sec. IV B, further work is needed to determine practical techniques for implementing an approximate swapping operator between the local motional modes and ion internal levels, including the assessment of many choices of the basis and the design of preconditioning procedures to strategically organize entanglement. Better understanding of successful procedures for imaging naturally distributed CV entanglement to finite dimensions may further inform the design of entanglement-efficient bosonic truncation and digitization schemes, e.g., in designing computational bases for the practical quantum simulation of quantum field theories [118,123,133–150].

The present connection between the scalar field vacuum and local motional modes of a trapped-ion chain, guided by entanglement structure, brings present research still closer to the vision of quantum simulation [20]: leveraging the mutual intersimulatability of diverse quantum systems, even those widely separated in natural energy scales, e.g., the

connection between atomic and subatomic physics arising in present quantum simulations of quantum chromodynamics.

ACKNOWLEDGMENTS

We thank R. Blatt, C. Noel, G. Pagano, M. J. Savage, and P. Zoller for inspiring discussions. The creative initiation of several aspects of this work occurred during the workshop ‘‘At the Interface of Quantum Sensors and Quantum Simulation’’ at the InQubator for Quantum Simulation (IQUS) hosted by the Institute for Nuclear Theory (INT). We thank R. Blatt and P. Zoller for challenging the organizers with homework throughout this workshop. D.H.B. is supported in part by National Science Foundation Nuclear Physics Grant No. PHY-2111046.

APPENDIX A: SMALL-CHAIN EXAMPLES

With a quadratic trapping potential, the equilibrium positions for two- and three-ion chains can be evaluated exactly to be

$$\begin{aligned} \mathbf{z}_{N=2}^0 &= \left\{ -\frac{2^{1/3}\ell_{\mu m}}{2}, \frac{2^{1/3}\ell_{\mu m}}{2} \right\}, \\ \mathbf{z}_{N=3}^0 &= \left\{ -\frac{10^{1/3}\ell_{\mu m}}{2}, 0, \frac{10^{1/3}\ell_{\mu m}}{2} \right\}, \end{aligned} \quad (\text{A1})$$

where $\ell_{\mu m} = (\frac{q}{8\pi\epsilon_0\kappa_2})^{1/3}$ is a characteristic ion-separation length scale. The resulting frequencies and normal modes are

$$\bar{\omega} = \frac{\omega}{\omega_z} = \{1, \sqrt{3}\}, \quad e = \begin{pmatrix} \mathbf{e}_1 \\ \mathbf{e}_2 \\ \mathbf{e}_3 \end{pmatrix} = \frac{1}{\sqrt{2}} \begin{pmatrix} 1 & 1 \\ -1 & 1 \end{pmatrix} \quad (\text{A2}) \quad \text{and}$$

$$\bar{\sigma}_{N=3} = \begin{pmatrix} \frac{29\sqrt{3}+\sqrt{145}+58}{174} & 0 & \frac{1}{3} - \frac{\sqrt{\frac{5}{29}}}{3} & 0 & \frac{-29\sqrt{3}+\sqrt{145}+58}{174} & 0 \\ 0 & \frac{15\sqrt{3}+\sqrt{145}+10}{30} & 0 & \frac{5-\sqrt{145}}{15} & 0 & \frac{-15\sqrt{3}+\sqrt{145}+10}{30} \\ \frac{1}{3} - \frac{\sqrt{\frac{5}{29}}}{3} & 0 & \frac{1}{3} + \frac{2\sqrt{\frac{5}{29}}}{3} & 0 & \frac{1}{3} - \frac{\sqrt{\frac{5}{29}}}{3} & 0 \\ 0 & \frac{5-\sqrt{145}}{15} & 0 & \frac{2\sqrt{145}+5}{15} & 0 & \frac{5-\sqrt{145}}{15} \\ \frac{-29\sqrt{3}+\sqrt{145}+58}{174} & 0 & \frac{1}{3} - \frac{\sqrt{\frac{5}{29}}}{3} & 0 & \frac{29\sqrt{3}+\sqrt{145}+58}{174} & 0 \\ 0 & \frac{-15\sqrt{3}+\sqrt{145}+10}{30} & 0 & \frac{5-\sqrt{145}}{15} & 0 & \frac{15\sqrt{3}+\sqrt{145}+10}{30} \end{pmatrix}. \quad (\text{A5})$$

As demonstrated in the second equation in Eq. (A4), restoring the dimensions of the CM is achieved, according to Eqs. (12) and (13), through insertion of ℓ_{nm}^2 or $\frac{\hbar^2}{\ell_{nm}^2}$ on the $\langle \hat{\phi} \hat{\phi} \rangle$ or $\langle \hat{\pi} \hat{\pi} \rangle$ submatrix, respectively. Note that the dimensionless covariance matrix of this harmonic approximation is universal; i.e., no trap or ion experimental parameters are present. Therefore, all entanglement properties are pure numbers, independent of the specifics of the chosen ion and strength of the quadratic trapping potential. In particular, the two-mode logarithmic negativities are found to be

$$\mathcal{N}_{1|2}^{N=2} = \frac{\ln 3}{\ln 16} = 0.396241 \dots, \quad (\text{A6})$$

$$\mathcal{N}_{1|2}^{N=3} = \frac{\ln \left(-\frac{5220}{-145(4\sqrt{3}+9)-2\sqrt{145}(11\sqrt{3}+153)+\sqrt{435(-5952\sqrt{3}+4(105\sqrt{3}+299)\sqrt{145}+13571)}} \right)}{\ln 4} = 0.384585 \dots, \quad (\text{A7})$$

$$\mathcal{N}_{1|3}^{N=3} = \frac{\ln \left(\frac{5}{3}(49 - 4\sqrt{145}) \right)}{\ln 16} = 0.118608 \dots, \quad (\text{A8})$$

where the third mode in the $N = 3$ examples has been traced. For the two-ion chain, the single-mode entanglement entropies are found to be

$$\begin{aligned} E_1^{N=2} &= \frac{1}{\ln 4096} \left\{ \left[\sqrt{6(2\sqrt{3}+3)+6} \right] \ln \left[\sqrt{6(2\sqrt{3}+3)+6} \right] \right. \\ &\quad \left. - 12 \ln 12 - \left[\sqrt{6(2\sqrt{3}+3)-6} \right] \ln \left[\sqrt{6(2\sqrt{3}+3)-6} \right] \right\} = 0.13618 \dots, \end{aligned} \quad (\text{A9})$$

for a two-ion chain and

$$\begin{aligned} \bar{\omega} &= \frac{\omega}{\omega_z} = \left\{ 1, \sqrt{3}, \sqrt{\frac{29}{5}} \right\}, \\ e &= \begin{pmatrix} \mathbf{e}_1 \\ \mathbf{e}_2 \\ \mathbf{e}_3 \end{pmatrix} = \begin{pmatrix} \frac{1}{\sqrt{3}} & \frac{1}{\sqrt{3}} & \frac{1}{\sqrt{3}} \\ -\frac{1}{\sqrt{2}} & 0 & \frac{1}{\sqrt{2}} \\ \frac{1}{\sqrt{6}} & -\frac{2}{\sqrt{6}} & \frac{1}{\sqrt{6}} \end{pmatrix} \end{aligned} \quad (\text{A3})$$

for a three-ion chain. Interestingly, the ground-state center-of-mass motion frequency and gap to the excited-state breathing mode are known to be independent of the number of ions in the chain [41].

With Eqs. (12)–(14), the dimensionless covariance matrices for two and three ions are directly calculated to be

$$\begin{aligned} \bar{\sigma}_{N=2} &= \frac{1}{2} \begin{pmatrix} \frac{3+\sqrt{3}}{3} & 0 & \frac{3-\sqrt{3}}{3} & 0 \\ 0 & 1+\sqrt{3} & 0 & 1-\sqrt{3} \\ \frac{3-\sqrt{3}}{3} & 0 & \frac{3+\sqrt{3}}{3} & 0 \\ 0 & 1-\sqrt{3} & 0 & 1+\sqrt{3} \end{pmatrix}, \\ \sigma_{N=2} &= \frac{\ell_{nm}^2}{2} \begin{pmatrix} \frac{3+\sqrt{3}}{3} & 0 & \frac{3-\sqrt{3}}{3} & 0 \\ 0 & \frac{\hbar^2(1+\sqrt{3})}{\ell_{nm}^4} & 0 & \frac{\hbar^2(1-\sqrt{3})}{\ell_{nm}^4} \\ \frac{3-\sqrt{3}}{3} & 0 & \frac{3+\sqrt{3}}{3} & 0 \\ 0 & \frac{\hbar^2(1-\sqrt{3})}{\ell_{nm}^4} & 0 & \frac{\hbar^2(1+\sqrt{3})}{\ell_{nm}^4} \end{pmatrix}, \end{aligned} \quad (\text{A4})$$

consistent with Ref. [76], in which the two-mode state of the local motional modes was taken to be a two-mode squeezed vacuum state in normal form, i.e., consistent with Eq. (A4) up to local operations.

APPENDIX B: LOCAL MOTIONAL MODES IN FOCK SPACE

A significant convenience of Gaussian CV quantum states is that they are completely described by a covariance matrix of second moments σ and a vector of first moments $\bar{\mathbf{r}}$ in phase space. The dimensionality of these two objects scales only linearly with the number of modes in the system, allowing states of significant size to be computationally practical. However, transferring entanglement from CV to finite-dimensional quantum systems, e.g., from local motional degrees of freedom to internal energy levels of trapped ions as first proposed in Ref. [76], inspires departing from the succinct phase-space language by expanding the CV state in the infinite tower of Fock states. From this basis, Ref. [76] discussed the experimental viability of dynamically swapping the lowest-excitation motional Fock states with an internal state ion qubit.

Before we evaluate the Fock-basis decomposition for an arbitrary covariance matrix, we consider first the Fock representation of a two-mode squeezed vacuum state [57],

$$|\psi_r\rangle = e^{r(\hat{a}_1^\dagger \hat{a}_2^\dagger - \hat{a}_1 \hat{a}_2)}|0, 0\rangle, \tag{B1}$$

where \hat{a}_j and \hat{a}_j^\dagger are bosonic creation and annihilation operators, $[\hat{a}_i, \hat{a}_j^\dagger] = \delta_{ij}$. As usual, the associated covariance matrix can be calculated via application of the two-mode squeezing symplectic operation to the vacuum (identity) covariance matrix,

$$\sigma_r = S_r S_r^T, \tag{B2}$$

$$S_r = \begin{pmatrix} \cosh r & 0 & \sinh r & 0 \\ 0 & \cosh r & 0 & -\sinh r \\ \sinh r & 0 & \cosh r & 0 \\ 0 & -\sinh r & 0 & \cosh r \end{pmatrix}.$$

The evaluation of Eq. (B1) can be performed by utilizing the $\text{su}(1,1)$ algebra, with generators K_\pm and K_0 satisfying the following commutation relations:

$$[K_+, K_-] = -2K_0, \quad [K_0, K_\pm] = \pm K_\pm. \tag{B3}$$

Transformations in this context can be simplified by using so-called disentanglement theorems [151,152],

$$e^{v_+ K_+ + v_- K_- + v_0 K_0} = e^{t_+ K_+} e^{(\ln t_0) K_0} e^{t_- K_-}. \tag{B4}$$

The determination of the coefficients \vec{t} from those of \vec{v} can be achieved by utilizing a small-dimensional representation of the generators—e.g., $K_+ = \begin{pmatrix} 0 & 1 \\ 0 & 0 \end{pmatrix}$, $K_- = \begin{pmatrix} 0 & 0 \\ -1 & 0 \end{pmatrix}$, and $K_0 = \frac{1}{2}Z$, with Z being the third Pauli matrix—and equating each matrix element of the two transformations. The resulting

coefficients are

$$t_0 = \left(\cosh(f) - \frac{v_0}{2f} \sinh(f) \right)^{-2}, \tag{B5}$$

$$t_\pm = \frac{v_\pm \sinh(f)}{f |\cosh(f) - \frac{v_0}{2f} \sinh(f)|}, \tag{B6}$$

with the parameter $f^2 = \frac{1}{4}v_0^2 - v_+v_-$. For application to the two-mode squeezed vacuum state, one may identify $K_+ = \hat{a}_1^\dagger \hat{a}_2^\dagger$ and $K_- = \hat{a}_1 \hat{a}_2$, leading to $K_0 = \frac{1}{2}(\hat{a}_1^\dagger \hat{a}_1 + \hat{a}_2^\dagger \hat{a}_2 + 1)$. The squeezing operation may thus be written in the well-known Fock-basis form,

$$e^{r(\hat{a}_1^\dagger \hat{a}_2^\dagger - \hat{a}_1 \hat{a}_2)}|0, 0\rangle = e^{\tanh(r)\hat{a}_1^\dagger \hat{a}_2^\dagger} e^{-(\ln \cosh r)(\hat{a}_1^\dagger \hat{a}_1 + \hat{a}_2^\dagger \hat{a}_2 + 1)} \times e^{-\tanh(r)\hat{a}_1 \hat{a}_2}|0, 0\rangle \tag{B7}$$

$$= \frac{1}{\cosh(r)} \sum_{n=0}^{\infty} \tanh^n(r) |n, n\rangle \tag{B8}$$

$$\equiv \sqrt{1 - e^{-2\beta}} \sum_{n=0}^{\infty} e^{-\beta n} |n, n\rangle, \tag{B9}$$

with $\beta \equiv -\ln \tanh(r)$ being commonly introduced. When acting on the vacuum state in Eq. (B7), only the identity survives from the first exponential on the right; the second exponential becomes simply a normalization factor, and the last exponential produces a tower of states with equal occupation and dominant support in the space of low excitations. As stronger squeezing is applied, the distribution in Fock space becomes increasingly delocalized, and the entanglement increases. For example, the logarithmic negativity, which is a necessary and sufficient measure of entanglement in this two-mode context, is directly proportional to the squeezing parameter as $\mathcal{N} = \frac{2|r|}{\ln 2}$.

For general Gaussian states, it is valuable to calculate Fock-basis density-matrix elements directly. Each Fock state, $|\mathbf{n}\rangle = (n_1, \dots, n_N)$, is labeled by a vector of numbers corresponding to the quantized excitations present in each of the N modes. With diagonal elements of the density matrix $\langle \mathbf{n} | \rho | \mathbf{n} \rangle$ commonly calculated for applications in Gaussian boson sampling [153,154], computational techniques for the generic matrix element $\langle \mathbf{m} | \rho | \mathbf{n} \rangle$ applicable to mixed quantum states were developed recently [155]. For states with $\bar{\mathbf{r}} = \mathbf{0}$, the techniques in Ref. [155] are summarized by the relations

$$\langle \mathbf{m} | \rho | \mathbf{n} \rangle = \frac{\text{haf}(\tilde{A})}{\sqrt{\det(\sigma_Q) \prod_{j=1}^N m_j! n_j!}}, \tag{B10}$$

$$\tilde{A} = \tilde{A} - \text{diag}(\tilde{A}), \quad A = X(\mathbb{I}_{2N} - \sigma_Q^{-1}),$$

with

$$X = \begin{pmatrix} 0 & \mathbb{I}_N \\ \mathbb{I}_N & 0 \end{pmatrix}, \quad \sigma_Q = \frac{1}{2}(U_{\hat{a}} \sigma_{xpp} U_{\hat{a}}^\dagger + \mathbb{I}_{2N}), \tag{B11}$$

$$U_{\hat{a}} = \frac{1}{\sqrt{2}} \begin{pmatrix} \mathbb{I}_N & i\mathbb{I}_N \\ \mathbb{I}_N & -i\mathbb{I}_N \end{pmatrix},$$

where U is the matrix transferring phase-space operators into bosonic creation and annihilation operators and σ_{xpp} is the position-momentum reordered covariance matrix according to the basis $\hat{\mathbf{r}}' = \{\hat{\phi}_1, \hat{\phi}_2, \dots, \hat{\phi}_N, \hat{\pi}_1, \hat{\pi}_2, \dots, \hat{\pi}_N\}$. Remaining

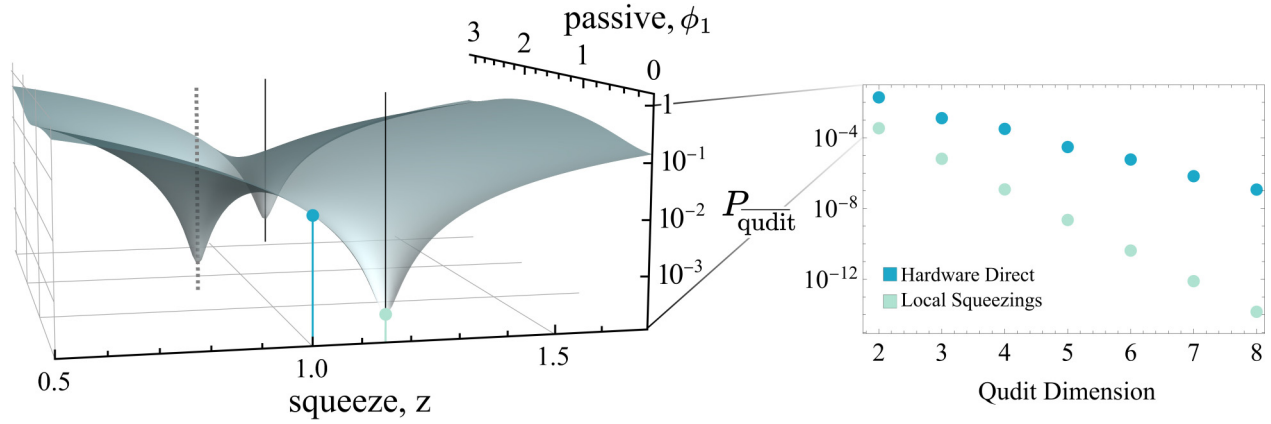


FIG. 5. Left: For the local motional modes of a two-ion chain, the probability outside the lowest two-level Fock subspace ($P_{\text{qudit}} = 1 - P_{\text{qubit}}$) is shown as a function of parameters governing one-mode symplectic operators applied symmetrically. That expressed directly by the hardware upon trapping without further operations, $(z, \phi_1) = (1, 0)$, is indicated in blue. The configurations optimally localizing the domain of support to this qubit-sized subspace are indicated by solid and dashed black lines, achieved by locally transforming the covariance matrix to normal form with constant diagonal $\langle \hat{\ell}_j \hat{\ell}_j \rangle = \langle \hat{\pi}_j \hat{\pi}_j \rangle$. Right: Scaling of probability outside the qudit subspace as a function of increasing Fock-space qudit dimension.

to be discussed are the Hafnian and \bar{A} . As usual, the Hafnian is a matrix property that can be calculated as

$$\text{haf}(B) = \sum_{\vec{j} \in \mathcal{M}} B_{j_1, j_2} \cdots B_{j_{n-1}, j_n}, \quad (\text{B12})$$

where \mathcal{M} is the set of all ways to partition the n elements of B into nonrepeating pairs. For example, $\text{haf}(B_{4 \times 4}) = B_{12}B_{34} + B_{13}B_{24} + B_{14}B_{23}$, and the Hafnian of an odd-dimensional matrix is zero. The Hafnian of a zero-dimensional matrix is set to be unity. While this computational form of the Hafnian makes manifest its combinatoric nature, note that Wick's theorem also allows $\text{haf}(B)$ to be calculated as a Gaussian expectation value of the product of all phase-space operators

subject to a covariance matrix governed by B and first moment displacements $\text{diag}(B)$. Finally, the matrix \bar{A} is constructed from A through repetition of its j th rows and columns n_j (m_j) times for the first (second) N dimensions to create a matrix of dimension $[\bar{A}] = \sum_j n_j + m_j$, scaling with the total number of Fock-space excitations involved in the matrix element.

Applying this formalism to the trapped-ion local motional modes, we consider the harmonic limit [Eq. (7)] of the two-ion system, characterized by the covariance matrix of Eq. (A4). In the Fock basis, the density-matrix elements for the first three levels in the basis of $\{|00\rangle, |01\rangle, |02\rangle, |10\rangle, |11\rangle, |12\rangle, |20\rangle, |21\rangle, |22\rangle\}$ will read

$$\bar{\rho}_{(0,1,2)} = \begin{pmatrix} 0.963 & 0 & \mathbf{-0.0913} & 0 & 0.129 & 0 & \mathbf{-0.0913} & 0 & 0.0259 \\ 0 & 0 & 0 & 0 & 0 & 0 & 0 & 0 & 0 \\ \mathbf{-0.0913} & 0 & \mathbf{0.00865} & 0 & \mathbf{-0.0122} & 0 & \mathbf{0.00865} & 0 & \mathbf{-0.00246} \\ 0 & 0 & 0 & 0 & 0 & 0 & 0 & 0 & 0 \\ 0.129 & 0 & \mathbf{-0.0122} & 0 & 0.0173 & 0 & \mathbf{-0.0122} & 0 & 0.00348 \\ 0 & 0 & 0 & 0 & 0 & 0 & 0 & 0 & 0 \\ \mathbf{-0.0913} & 0 & \mathbf{0.00865} & 0 & \mathbf{-0.0122} & 0 & \mathbf{0.00865} & 0 & \mathbf{-0.00246} \\ 0 & 0 & 0 & 0 & 0 & 0 & 0 & 0 & 0 \\ 0.0259 & 0 & \mathbf{-0.00246} & 0 & 0.00348 & 0 & \mathbf{-0.00246} & 0 & 0.000698 \end{pmatrix}. \quad (\text{B13})$$

Note that, as a subset, this portion of the density matrix is neither pure nor normalized. The presence of the bold elements is a clear indication that the two-ion state of local motional modes is not simply a two-mode squeezed vacuum state, Eq. (B9), as presented in Ref. [76]. However, one can transform the two-ion local motional modes into a two-mode squeezed vacuum state through local symplectic operations, leading to agreement with the reported entanglement properties for the two-ion system.

While the presence of local operations does not impact the value of entanglement measures, it does impact the distribution of a CV quantum state in Fock space. If aims of entanglement extraction from the local motional modes to the ion internal levels are pursued through exchange with the lowest Fock states, as first proposed by Ref. [76], it is important to ensure dominant support is present in this low-occupation Hilbert subspace. For a two-ion chain, the left panel of Fig. 5 demonstrates the deviation of this probability from unity

P_{qubit}^{-} , i.e., the probability of the local motional modes being outside the two-state subspace of Fock states $|0\rangle$ and $|1\rangle$ as a function of local operations. To parametrize single-mode symplectic operations, one may perform a rudimentary application of the Bloch-Messiah decomposition, allowing a symplectic transformation to be decomposed into a set of single-mode squeezing (Z) operations surrounded by a pair of passive (O) operations (energy-preserving, e.g., beam splitters and phase shifters), with real numbers (ϕ_1, ϕ_2, z) as [57,156,157]

$$S = O_1 Z O_2,$$

$$O_j = \begin{pmatrix} \text{Re}(\gamma_j) & \text{Im}(\gamma_j) \\ -\text{Im}(\gamma_j) & \text{Re}(\gamma_j) \end{pmatrix}, \quad Z = \begin{pmatrix} z & 0 \\ 0 & \frac{1}{z} \end{pmatrix}, \quad (\text{B14})$$

where $\gamma_j = e^{i\phi_j}$ is a one-dimensional unitary. When each local motional mode is squeezed by $z = (\sigma_{2,2}/\sigma_{1,1})^{1/4}$, the quantum

state upon trapping of an ion pair (blue point in Fig. 5) can be shifted to a form that optimally compacts the support of the quantum state in the low Fock states (green point and solid line). The alternate solution (dashed line) simply exchanges the position and momentum components, and thus, both optimal points yield a two-mode squeezed vacuum state with the Fock basis characterized by Eq. (B9). It is anticipated that this determination of the true form of the local motional mode CV quantum state and its guidance for additional single-mode squeezing operations will improve experimental implementations of ion motional entanglement extraction.

APPENDIX C: NUMERICAL TABLES

Tables I–VII provide numerical values presented in Figs. 3 and 4 in the main text and Fig. 5 in Appendix B.

TABLE I. Numerical values for A, B region sizes of one ion or lattice site in Fig. 3.

Separation \tilde{r}/d	Ions			Scalar		
	$\mathcal{N}_{A B}(\sigma^{(l)})$	$\mathcal{N}_{A B}(\sigma^{(m,\phi)})$	$\mathcal{N}_{A B}(\sigma^{(m,\pi)})$	$\mathcal{N}_{A B}(\sigma^{(l)})$	$\mathcal{N}_{A B}(\sigma^{(m,\phi)})$	$\mathcal{N}_{A B}(\sigma^{(m,\pi)})$
0	3.66×10^{-1}	3.94×10^{-1}	9.25×10^{-1}	4.44×10^{-1}	5.00×10^{-1}	2.30
1	5.95×10^{-2}	1.14×10^{-1}	7.38×10^{-1}	0	9.63×10^{-2}	2.08
2	0	5.48×10^{-2}	6.43×10^{-1}	0	4.12×10^{-2}	1.97
3	0	3.25×10^{-2}	5.81×10^{-1}	0	2.29×10^{-2}	1.90
4	0	2.16×10^{-2}	5.36×10^{-1}	0	1.46×10^{-2}	1.85
5	0	1.54×10^{-2}	5.00×10^{-1}	0	1.01×10^{-2}	1.81
6	0	1.16×10^{-2}	4.71×10^{-1}	0	7.40×10^{-3}	1.78
7	0	9.04×10^{-3}	4.46×10^{-1}	0	5.66×10^{-3}	1.76
8	0	7.26×10^{-3}	4.25×10^{-1}	0	4.47×10^{-3}	1.73
9	0	5.97×10^{-3}	4.06×10^{-1}	0	3.62×10^{-3}	1.71
10	0	4.99×10^{-3}	3.90×10^{-1}	0	2.99×10^{-3}	1.70

TABLE II. Numerical values for A, B region sizes of three ions or lattice sites in Fig. 3.

Separation \tilde{r}/d	Ions			Scalar		
	$\mathcal{N}_{A B}(\sigma^{(l)})$	$\mathcal{N}_{A B}(\sigma^{(m,\phi)})$	$\mathcal{N}_{A B}(\sigma^{(m,\pi)})$	$\mathcal{N}_{A B}(\sigma^{(l)})$	$\mathcal{N}_{A B}(\sigma^{(m,\phi)})$	$\mathcal{N}_{A B}(\sigma^{(m,\pi)})$
0	6.29×10^{-1}	6.73×10^{-1}	1.22	7.89×10^{-1}	8.39×10^{-1}	2.71
$\frac{1}{3}$	2.01×10^{-1}	2.47×10^{-1}	9.91×10^{-1}	1.68×10^{-1}	2.19×10^{-1}	2.43
$\frac{2}{3}$	6.77×10^{-2}	1.40×10^{-1}	8.73×10^{-1}	2.77×10^{-2}	1.14×10^{-1}	2.29
1	1.27×10^{-2}	9.25×10^{-2}	7.95×10^{-1}	4.41×10^{-3}	7.21×10^{-2}	2.20
$\frac{4}{3}$	2.96×10^{-3}	6.65×10^{-2}	7.36×10^{-1}	2.07×10^{-3}	5.03×10^{-2}	2.14
$\frac{5}{3}$	1.45×10^{-3}	5.05×10^{-2}	6.90×10^{-1}	1.19×10^{-3}	3.73×10^{-2}	2.09
2	8.58×10^{-4}	3.98×10^{-2}	6.52×10^{-1}	6.99×10^{-4}	2.88×10^{-2}	2.05
$\frac{7}{3}$	5.31×10^{-4}	3.23×10^{-2}	6.19×10^{-1}	3.86×10^{-4}	2.30×10^{-2}	2.02
$\frac{8}{3}$	3.20×10^{-4}	2.68×10^{-2}	5.91×10^{-1}	1.65×10^{-4}	1.88×10^{-2}	1.99
3	1.71×10^{-4}	2.26×10^{-2}	5.66×10^{-1}	0	1.57×10^{-2}	1.96
$\frac{10}{3}$	5.99×10^{-5}	1.93×10^{-2}	5.44×10^{-1}	0	1.33×10^{-2}	1.94
$\frac{11}{3}$	0	1.67×10^{-2}	5.24×10^{-1}	0	1.14×10^{-2}	1.92
4	0	1.46×10^{-2}	5.06×10^{-1}	0	9.88×10^{-3}	1.90
$\frac{13}{3}$	0	1.29×10^{-2}	4.89×10^{-1}	0	8.65×10^{-3}	1.89
$\frac{14}{3}$	0	1.15×10^{-2}	4.74×10^{-1}	0	7.64×10^{-3}	1.87
5	0	1.03×10^{-2}	4.59×10^{-1}	0	6.80×10^{-3}	1.86
$\frac{16}{3}$	0	9.28×10^{-3}	4.46×10^{-1}	0	6.09×10^{-3}	1.85
$\frac{17}{3}$	0	8.41×10^{-3}	4.33×10^{-1}	0	5.49×10^{-3}	1.83
6	0	7.66×10^{-3}	4.22×10^{-1}	0	4.97×10^{-3}	1.82
$\frac{19}{3}$	0	7.01×10^{-3}	4.10×10^{-1}	0	4.53×10^{-3}	1.81
$\frac{20}{3}$	0	6.43×10^{-3}	4.00×10^{-1}	0	4.14×10^{-3}	1.80
7	0	5.93×10^{-3}	3.90×10^{-1}	0	3.80×10^{-3}	1.79
$\frac{22}{3}$	0	5.48×10^{-3}	3.81×10^{-1}	0	3.50×10^{-3}	1.78
$\frac{23}{3}$	0	5.09×10^{-3}	3.72×10^{-1}	0	3.23×10^{-3}	1.78
8	0	4.73×10^{-3}	3.63×10^{-1}	0	2.99×10^{-3}	1.77
$\frac{25}{3}$	0	4.41×10^{-3}	3.55×10^{-1}	0	2.78×10^{-3}	1.76
$\frac{26}{3}$	0	4.13×10^{-3}	3.47×10^{-1}	0	2.59×10^{-3}	1.75
9	0	3.87×10^{-3}	3.39×10^{-1}	0	2.42×10^{-3}	1.75

TABLE III. Numerical values for A, B region sizes of five ions or lattice sites in Fig. 3.

Separation \tilde{r}/d	Ions			Scalar		
	$\mathcal{N}_{A B}(\sigma^{(l)})$	$\mathcal{N}_{A B}(\sigma^{(m,\phi)})$	$\mathcal{N}_{A B}(\sigma^{(m,\pi)})$	$\mathcal{N}_{A B}(\sigma^{(l)})$	$\mathcal{N}_{A B}(\sigma^{(m,\phi)})$	$\mathcal{N}_{A B}(\sigma^{(m,\pi)})$
0	7.75×10^{-1}	8.18×10^{-1}	1.33	9.67×10^{-1}	1.01	2.89
$\frac{1}{5}$	2.89×10^{-1}	3.32×10^{-1}	1.09	2.55×10^{-1}	3.00×10^{-1}	2.59
$\frac{2}{5}$	1.32×10^{-1}	2.02×10^{-1}	9.69×10^{-1}	8.55×10^{-2}	1.71×10^{-1}	2.44
$\frac{3}{5}$	5.77×10^{-2}	1.41×10^{-1}	8.85×10^{-1}	2.87×10^{-2}	1.15×10^{-1}	2.35
$\frac{4}{5}$	2.36×10^{-2}	1.06×10^{-1}	8.22×10^{-1}	1.40×10^{-2}	8.42×10^{-2}	2.28
1	1.17×10^{-2}	8.32×10^{-2}	7.72×10^{-1}	8.53×10^{-3}	6.48×10^{-2}	2.22
$\frac{6}{5}$	7.11×10^{-3}	6.74×10^{-2}	7.30×10^{-1}	5.66×10^{-3}	5.17×10^{-2}	2.18
$\frac{7}{5}$	4.74×10^{-3}	5.60×10^{-2}	6.95×10^{-1}	3.86×10^{-3}	4.24×10^{-2}	2.14
$\frac{8}{5}$	3.30×10^{-3}	4.73×10^{-2}	6.64×10^{-1}	2.63×10^{-3}	3.54×10^{-2}	2.11
$\frac{9}{5}$	2.32×10^{-3}	4.06×10^{-2}	6.37×10^{-1}	1.73×10^{-3}	3.01×10^{-2}	2.08
2	1.62×10^{-3}	3.53×10^{-2}	6.13×10^{-1}	1.06×10^{-3}	2.59×10^{-2}	2.06
$\frac{11}{5}$	1.09×10^{-3}	3.10×10^{-2}	5.91×10^{-1}	5.78×10^{-4}	2.26×10^{-2}	2.04
$\frac{12}{5}$	6.87×10^{-4}	2.74×10^{-2}	5.70×10^{-1}	2.65×10^{-4}	1.98×10^{-2}	2.02
$\frac{13}{5}$	3.86×10^{-4}	2.45×10^{-2}	5.52×10^{-1}	9.64×10^{-5}	1.76×10^{-2}	2.00
$\frac{14}{5}$	1.83×10^{-4}	2.20×10^{-2}	5.35×10^{-1}	2.62×10^{-5}	1.57×10^{-2}	1.98
3	6.87×10^{-5}	1.99×10^{-2}	5.19×10^{-1}	9.51×10^{-6}	1.41×10^{-2}	1.97
$\frac{16}{5}$	2.00×10^{-5}	1.80×10^{-2}	5.04×10^{-1}	5.13×10^{-6}	1.27×10^{-2}	1.95
$\frac{17}{5}$	7.42×10^{-6}	1.65×10^{-2}	4.90×10^{-1}	3.28×10^{-6}	1.16×10^{-2}	1.94
$\frac{18}{5}$	4.01×10^{-6}	1.51×10^{-2}	4.77×10^{-1}	2.27×10^{-6}	1.05×10^{-2}	1.93
$\frac{19}{5}$	2.59×10^{-6}	1.39×10^{-2}	4.65×10^{-1}	1.63×10^{-6}	9.66×10^{-3}	1.91
4	1.82×10^{-6}	1.28×10^{-2}	4.53×10^{-1}	1.18×10^{-6}	8.88×10^{-3}	1.90
$\frac{21}{5}$	1.33×10^{-6}	1.19×10^{-2}	4.42×10^{-1}	8.56×10^{-7}	8.20×10^{-3}	1.89
$\frac{22}{5}$	9.99×10^{-7}	1.10×10^{-2}	4.32×10^{-1}	6.05×10^{-7}	7.59×10^{-3}	1.88
$\frac{23}{5}$	7.55×10^{-7}	1.03×10^{-2}	4.21×10^{-1}	4.05×10^{-7}	7.05×10^{-3}	1.87
$\frac{24}{5}$	5.69×10^{-7}	9.61×10^{-3}	4.12×10^{-1}	2.41×10^{-7}	6.56×10^{-3}	1.87
5	4.21×10^{-7}	9.00×10^{-3}	4.03×10^{-1}	1.05×10^{-7}	6.12×10^{-3}	1.86
$\frac{26}{5}$	3.01×10^{-7}	8.45×10^{-3}	3.94×10^{-1}	0	5.73×10^{-3}	1.85
$\frac{27}{5}$	2.01×10^{-7}	7.94×10^{-3}	3.85×10^{-1}	0	5.37×10^{-3}	1.84
$\frac{28}{5}$	1.17×10^{-7}	7.48×10^{-3}	3.77×10^{-1}	0	5.04×10^{-3}	1.83
$\frac{29}{5}$	4.50×10^{-8}	7.07×10^{-3}	3.69×10^{-1}	0	4.75×10^{-3}	1.83
6	0	6.68×10^{-3}	3.62×10^{-1}	0	4.48×10^{-3}	1.82
$\frac{31}{5}$	0	6.33×10^{-3}	3.55×10^{-1}	0	4.23×10^{-3}	1.81
$\frac{32}{5}$	0	6.00×10^{-3}	3.48×10^{-1}	0	4.00×10^{-3}	1.81
$\frac{33}{5}$	0	5.70×10^{-3}	3.41×10^{-1}	0	3.79×10^{-3}	1.80
$\frac{34}{5}$	0	5.43×10^{-3}	3.34×10^{-1}	0	3.59×10^{-3}	1.80
7	0	5.17×10^{-3}	3.28×10^{-1}	0	3.42×10^{-3}	1.79
$\frac{36}{5}$	0	4.93×10^{-3}	3.22×10^{-1}	0	3.25×10^{-3}	1.78
$\frac{37}{5}$	0	4.71×10^{-3}	3.16×10^{-1}	0	3.10×10^{-3}	1.78
$\frac{38}{5}$	0	4.50×10^{-3}	3.10×10^{-1}	0	2.95×10^{-3}	1.77
$\frac{39}{5}$	0	4.30×10^{-3}	3.04×10^{-1}	0	2.82×10^{-3}	1.77
8	0	4.12×10^{-3}	2.99×10^{-1}	0	2.69×10^{-3}	1.76
$\frac{41}{5}$	0	3.95×10^{-3}	2.93×10^{-1}	0	2.58×10^{-3}	1.76
$\frac{42}{5}$	0	3.79×10^{-3}	2.88×10^{-1}	0	2.47×10^{-3}	1.75
$\frac{43}{5}$	0	3.65×10^{-3}	2.83×10^{-1}	0	2.36×10^{-3}	1.75
$\frac{44}{5}$	0	3.50×10^{-3}	2.78×10^{-1}	0	2.27×10^{-3}	1.75
9	0	3.37×10^{-3}	2.73×10^{-1}	0	2.18×10^{-3}	1.74

TABLE IV. Numerical values for the $N = 30$ ion chain shown in Fig. 4.

Region size	Squeezing z	Fidelity	
		Raw	Locally squeezed
2	4.119	3.49×10^{-1}	0.814
4	3.666	1.88×10^{-1}	0.767
6	3.507	1.03×10^{-1}	0.738
8	3.420	5.79×10^{-2}	0.717
10	3.362	3.28×10^{-2}	0.699
12	3.315	1.89×10^{-2}	0.682
14	3.274	1.10×10^{-2}	0.667
16	3.234	6.56×10^{-3}	0.652
18	3.194	3.99×10^{-3}	0.636
20	3.152	2.49×10^{-3}	0.619
22	3.106	1.60×10^{-3}	0.600
24	3.054	1.08×10^{-3}	0.576
26	2.993	7.59×10^{-4}	0.544
28	2.919	5.73×10^{-4}	0.493
30	2.821	4.47×10^{-4}	0.368

TABLE V. Numerical values for the $N = 50$ ion chain shown in Fig. 4.

Region size	Squeezing z	Fidelity	
		Raw	Locally squeezed
2	5.118	2.83×10^{-1}	0.827
4	4.579	1.25×10^{-1}	0.784
6	4.390	5.70×10^{-2}	0.758
8	4.292	2.62×10^{-2}	0.739
10	4.229	1.22×10^{-2}	0.724
12	4.184	5.67×10^{-3}	0.710
14	4.149	2.67×10^{-3}	0.698
16	4.118	1.26×10^{-3}	0.686
18	4.091	6.04×10^{-4}	0.675
20	4.066	2.91×10^{-4}	0.665
22	4.041	1.42×10^{-4}	0.654
24	4.016	6.97×10^{-5}	0.644
26	3.991	3.47×10^{-5}	0.634
28	3.965	1.75×10^{-5}	0.624
30	3.938	9.00×10^{-6}	0.613
32	3.910	4.70×10^{-6}	0.601
34	3.879	2.51×10^{-6}	0.588
36	3.846	1.37×10^{-6}	0.574
38	3.811	7.67×10^{-7}	0.557
40	3.771	4.44×10^{-7}	0.538
42	3.728	2.66×10^{-7}	0.515
44	3.679	1.67×10^{-7}	0.485
46	3.623	1.12×10^{-7}	0.445
48	3.556	8.03×10^{-8}	0.387
50	3.473	6.09×10^{-8}	0.271

TABLE VI. Numerical values for the $N = 150$ ion chain shown in Fig. 4.

Region size	Squeezing z	Fidelity	
		Raw	Locally squeezed
2	8.262	1.73×10^{-1}	0.850
4	7.453	4.86×10^{-2}	0.813
6	7.166	1.40×10^{-2}	0.792
8	7.018	4.08×10^{-3}	0.776
10	6.928	1.19×10^{-3}	0.763
12	6.866	3.51×10^{-4}	0.752
14	6.821	1.03×10^{-4}	0.742
16	6.787	3.06×10^{-5}	0.733
18	6.759	9.05×10^{-6}	0.724
20	6.736	2.68×10^{-6}	0.716
22	6.716	7.98×10^{-7}	0.709
24	6.699	2.37×10^{-7}	0.701
26	6.684	7.08×10^{-8}	0.694
28	6.671	2.12×10^{-8}	0.688
30	6.658	6.34×10^{-9}	0.681
32	6.646	1.90×10^{-9}	0.675
34	6.635	5.71×10^{-10}	0.669
36	6.625	1.72×10^{-10}	0.663
38	6.615	5.19×10^{-11}	0.657
40	6.605	1.57×10^{-11}	0.652
42	6.596	4.76×10^{-12}	0.646
44	6.586	1.45×10^{-12}	0.640
46	6.577	4.41×10^{-13}	0.635
48	6.568	1.35×10^{-13}	0.630
50	6.558	4.12×10^{-14}	0.624

TABLE VII. Numerical values shown in Fig. 5.

Fock truncation/qudit dimension	P_{qudit}	
	Raw	Locally squeezed
2	1.93×10^{-2}	3.47×10^{-4}
3	1.28×10^{-3}	6.46×10^{-6}
4	3.17×10^{-4}	1.20×10^{-7}
5	2.99×10^{-5}	2.24×10^{-9}
6	5.88×10^{-6}	4.17×10^{-11}
7	6.73×10^{-7}	7.77×10^{-13}
8	1.17×10^{-7}	1.45×10^{-14}

- [1] C. M. Ho and S. D. H. Hsu, Entanglement and fast quantum thermalization in heavy ion collisions, *Mod. Phys. Lett. A* **31**, 1650110 (2016).
- [2] A. M. Kaufman, M. E. Tai, A. Lukin, M. Rispoli, R. Schittko, P. M. Preiss, and M. Greiner, Quantum thermalization through entanglement in an isolated many-body system, *Science* **353**, 794 (2016).
- [3] D. E. Kharzeev and E. M. Levin, Deep inelastic scattering as a probe of entanglement, *Phys. Rev. D* **95**, 114008 (2017).
- [4] O. K. Baker and D. E. Kharzeev, Thermal radiation and entanglement in proton-proton collisions at energies available at the CERN Large Hadron Collider, *Phys. Rev. D* **98**, 054007 (2018).
- [5] A. Cervera-Lierta, J. I. Latorre, J. Rojo, and L. Rottoli, Maximal entanglement in high energy physics, *SciPost Phys.* **3**, 036 (2017).
- [6] J. Berges, S. Floerchinger, and R. Venugopalan, Entanglement and thermalization, *Nucl. Phys. A* **982**, 819 (2019).
- [7] S. R. Beane, D. B. Kaplan, N. Klco, and M. J. Savage, Entanglement suppression and emergent symmetries of strong interactions, *Phys. Rev. Lett.* **122**, 102001 (2019).
- [8] C. W. Johnson and O. C. Gorton, Proton-neutron entanglement in the nuclear shell model, *J. Phys. G: Nucl. Part. Phys.* **50**, 045110 (2023).
- [9] S. R. Beane and P. Ehlers, Chiral symmetry breaking, entanglement, and the nucleon spin decomposition, *Mod. Phys. Lett. A* **35**, 2050048 (2020).
- [10] Z. Tu, D. E. Kharzeev, and T. Ullrich, Einstein-Podolsky-Rosen paradox and quantum entanglement at subnucleonic scales, *Phys. Rev. Lett.* **124**, 062001 (2020).
- [11] S. R. Beane and R. C. Farrell, Geometry and entanglement in the scattering matrix, *Ann. Phys. (NY)* **433**, 168581 (2021).
- [12] S. R. Beane, R. C. Farrell, and M. Varma, Entanglement minimization in hadronic scattering with pions, *Int. J. Mod. Phys. A* **36**, 2150205 (2021).
- [13] D. E. Kharzeev and E. Levin, Deep inelastic scattering as a probe of entanglement: Confronting experimental data, *Phys. Rev. D* **104**, L031503 (2021).
- [14] C. Robin, M. J. Savage, and N. Pillet, Entanglement rearrangement in self-consistent nuclear structure calculations, *Phys. Rev. C* **103**, 034325 (2021).
- [15] I. Low and T. Mehen, Symmetry from entanglement suppression, *Phys. Rev. D* **104**, 074014 (2021).
- [16] W. Gong, G. Parida, Z. Tu, and R. Venugopalan, Measurement of Bell-type inequalities and quantum entanglement from Λ -hyperon spin correlations at high energy colliders, *Phys. Rev. D* **106**, L031501 (2022).
- [17] A. Roggero, Entanglement and many-body effects in collective neutrino oscillations, *Phys. Rev. D* **104**, 103016 (2021).
- [18] N. Mueller, T. V. Zache, and R. Ott, Thermalization of gauge theories from their entanglement spectrum, *Phys. Rev. Lett.* **129**, 011601 (2022).
- [19] M. K. Joshi, C. Kokail, R. van Bijnen, F. Kranzl, T. V. Zache, R. Blatt, C. F. Roos, and P. Zoller, Exploring large-scale entanglement in quantum simulation, *Nature (London)* **624**, 539 (2023).
- [20] R. P. Feynman, Simulating physics with computers, *Int. J. Theor. Phys.* **21**, 467 (1982).
- [21] M. B. Plenio and S. Virmani, An introduction to entanglement measures, *Quantum Inf. Comput.* **7**, 001 (2007).
- [22] M. A. Nielsen and I. L. Chuang, *Quantum Computation and Quantum Information* (Cambridge University Press, Cambridge, 2010).
- [23] R. Horodecki, P. Horodecki, M. Horodecki, and K. Horodecki, Quantum entanglement, *Rev. Mod. Phys.* **81**, 865 (2009).
- [24] M. M. Wilde, *Quantum Information Theory* (Cambridge University Press, Cambridge, 2013).
- [25] C. L. Degen, F. Reinhard, and P. Cappellaro, Quantum sensing, *Rev. Mod. Phys.* **89**, 035002 (2017).
- [26] N. Klco, A. Roggero, and M. J. Savage, Standard model physics and the digital quantum revolution: Thoughts about the interface, *Rep. Prog. Phys.* **85**, 064301 (2022).
- [27] R. Kaubruegger, D. V. Vasilyev, M. Schulte, K. Hammerer, and P. Zoller, Quantum variational optimization of Ramsey interferometry and atomic clocks, *Phys. Rev. X* **11**, 041045 (2021).
- [28] C. D. Marciniak, T. Feldker, I. Pogorelov, R. Kaubruegger, D. V. Vasilyev, R. van Bijnen, P. Schindler, P. Zoller, R. Blatt, and T. Monz, Optimal metrology with programmable quantum sensors, *Nature (London)* **603**, 604 (2022).
- [29] E. Altman, K. R. Brown, G. Carleo, L. D. Carr, E. Demler, C. Chin, B. DeMarco, S. E. Economou, M. A. Eriksson, K.-M. C. Fu *et al.*, Quantum simulators: Architectures and opportunities, *PRX Quantum* **2**, 017003 (2021).
- [30] A. J. Daley, I. Bloch, C. Kokail, S. Flannigan, N. Pearson, M. Troyer, and P. Zoller, Practical quantum advantage in quantum simulation, *Nature (London)* **607**, 667 (2022).
- [31] A. J. Brady, C. Gao, R. Harnik, Z. Liu, Z. Zhang, and Q. Zhuang, Entangled sensor-networks for dark-matter searches, *PRX Quantum* **3**, 030333 (2022).
- [32] H. Reeh and S. Schlieder, Bemerkungen zur unitäräquivalenz von lorentzinvarianten feldern, *Nuovo Cimento* **22**, 1051 (1961).
- [33] S. J. Summers and R. Werner, The vacuum violates Bell's inequalities, *Phys. Lett. A* **110**, 257 (1985).
- [34] S. J. Summers and R. Werner, Bell's inequalities and quantum field theory. I. General setting, *J. Math. Phys.* **28**, 2440 (1987).
- [35] S. J. Summers and R. Werner, Bell's inequalities and quantum field theory. II. Bell's inequalities are maximally violated in the vacuum, *J. Math. Phys.* **28**, 2448 (1987).
- [36] H. Halvorson and R. Clifton, Generic Bell correlation between arbitrary local algebras in quantum field theory, *J. Math. Phys.* **41**, 1711 (2000).
- [37] A. Valentini, Non-local correlations in quantum electrodynamics, *Phys. Lett. A* **153**, 321 (1991).
- [38] B. Reznik, Entanglement from the vacuum, *Found. Phys.* **33**, 167 (2003).
- [39] B. Reznik, A. Retzker, and J. Silman, Violating Bell's inequalities in the vacuum, *Phys. Rev. A* **71**, 042104 (2005).
- [40] W. Chen, J. Gan, J.-N. Zhang, D. Matuskevich, and K. Kim, Quantum computation and simulation with vibrational modes of trapped ions, *Chin. Phys. B* **30**, 060311 (2021).
- [41] J. I. Cirac and P. Zoller, Quantum computations with cold trapped ions, *Phys. Rev. Lett.* **74**, 4091 (1995).
- [42] C. Monroe, D. M. Meekhof, B. E. King, W. M. Itano, and D. J. Wineland, Demonstration of a fundamental quantum logic gate, *Phys. Rev. Lett.* **75**, 4714 (1995).
- [43] A. Sørensen and K. Mølmer, Quantum computation with ions in thermal motion, *Phys. Rev. Lett.* **82**, 1971 (1999).

- [44] D. Leibfried, B. DeMarco, V. Meyer, D. Lucas, M. Barrett, J. Britton, W. Itano, B. Jelenković, C. Langer, T. Rosenband, and D. Wineland, Experimental demonstration of a robust, high-fidelity geometric two ion-qubit phase gate, *Nature (London)* **422**, 412 (2003).
- [45] F. Schmidt-Kaler, H. Häffner, M. Riebe, S. Gulde, G. P. T. Lancaster, T. Deuschle, C. Becher, C. F. Roos, J. Eschner, and R. Blatt, Realization of the Cirac-Zoller controlled-not quantum gate, *Nature (London)* **422**, 408 (2003).
- [46] O. Katz, M. Cetina, and C. Monroe, Programmable N-body interactions with trapped ions, *PRX Quantum* **4**, 030311 (2023).
- [47] J. Casanova, L. Lamata, I. L. Egusquiza, R. Gerritsma, C. F. Roos, J. J. Garcia-Ripoll, and E. Solano, Quantum simulation of quantum field theories in trapped ions, *Phys. Rev. Lett.* **107**, 260501 (2011).
- [48] Z. Davoudi, N. M. Linke, and G. Pagano, Toward simulating quantum field theories with controlled phonon-ion dynamics: A hybrid analog-digital approach, *Phys. Rev. Res.* **3**, 043072 (2021).
- [49] N. Klco and D. H. Beck, Entanglement structures in quantum field theories. II. Distortions of vacuum correlations through the lens of local observers, *Phys. Rev. A* **108**, 012429 (2023).
- [50] M. G. Raizen, J. M. Gilligan, J. C. Bergquist, W. M. Itano, and D. J. Wineland, Ionic crystals in a linear Paul trap, *Phys. Rev. A* **45**, 6493 (1992).
- [51] D. J. Wineland, C. Monroe, W. M. Itano, D. Leibfried, B. E. King, and D. M. Meekhof, Experimental issues in coherent quantum state manipulation of trapped atomic ions, *J. Res. Natl. Inst. Stand. Technol.* **103**, 259 (1998).
- [52] G. D. Lin, S. L. Zhu, R. Islam, K. Kim, M. S. Chang, S. Korenblit, C. Monroe, and L. M. Duan, Large-scale quantum computation in an anharmonic linear ion trap, *Europhys. Lett.* **86**, 60004 (2009).
- [53] J. P. Home, D. Hanneke, J. D. Jost, D. Leibfried, and D. J. Wineland, Normal modes of trapped ions in the presence of anharmonic trap potentials, *New J. Phys.* **13**, 073026 (2011).
- [54] A. M. Steane, The ion trap quantum information processor, *Appl. Phys. B* **64**, 623 (1997).
- [55] D. F. V. James, Quantum dynamics of cold trapped ions with application to quantum computation, *Appl. Phys. B* **66**, 181 (1998).
- [56] S. L. Braunstein and P. van Loock, Quantum information with continuous variables, *Rev. Mod. Phys.* **77**, 513 (2005).
- [57] A. Serafini, *Quantum Continuous Variables: A Primer of Theoretical Methods* (CRC Press, Boca Raton, FL, 2017).
- [58] J. Williamson, On the algebraic problem concerning the normal forms of linear dynamical systems, *Am. J. Math.* **58**, 141 (1936).
- [59] A. Botero and B. Reznik, Modewise entanglement of Gaussian states, *Phys. Rev. A* **67**, 052311 (2003).
- [60] N. Klco, D. H. Beck, and M. J. Savage, Entanglement structures in quantum field theories: Negativity cores and bound entanglement in the vacuum, *Phys. Rev. A* **107**, 012415 (2023).
- [61] S. Marcovitch, A. Retzker, M. B. Plenio, and B. Reznik, Critical and noncritical long-range entanglement in Klein-Gordon fields, *Phys. Rev. A* **80**, 012325 (2009).
- [62] N. Klco and M. J. Savage, Geometric quantum information structure in quantum fields and their lattice simulation, *Phys. Rev. D* **103**, 065007 (2021).
- [63] N. Klco and M. J. Savage, Entanglement spheres and a UV-IR connection in effective field theories, *Phys. Rev. Lett.* **127**, 211602 (2021).
- [64] K. Audenaert, J. Eisert, M. B. Plenio, and R. F. Werner, Entanglement properties of the harmonic chain, *Phys. Rev. A* **66**, 042327 (2002).
- [65] A. Botero and B. Reznik, Spatial structures and localization of vacuum entanglement in the linear harmonic chain, *Phys. Rev. A* **70**, 052329 (2004).
- [66] J. Kofler, V. Vedral, M. S. Kim, and Č. Brukner, Entanglement between collective operators in a linear harmonic chain, *Phys. Rev. A* **73**, 052107 (2006).
- [67] P. Calabrese, J. Cardy, and E. Tonni, Entanglement entropy of two disjoint intervals in conformal field theory, *J. Stat. Mech.* (2009) P11001.
- [68] P. Calabrese, J. Cardy, and E. Tonni, Entanglement negativity in quantum field theory, *Phys. Rev. Lett.* **109**, 130502 (2012).
- [69] P. Calabrese, J. Cardy, and E. Tonni, Entanglement negativity in extended systems: A field theoretical approach, *J. Stat. Mech.* (2013) P02008.
- [70] M. R. Mohammadi Mozaffar and A. Mollabashi, Entanglement in Lifshitz-type quantum field theories, *J. High Energy Phys.* **07** (2017) 120.
- [71] A. Coser, C. De Nobili, and E. Tonni, A contour for the entanglement entropies in harmonic lattices, *J. Phys. A* **50**, 314001 (2017).
- [72] Y. Javanmard, D. Trapin, S. Bera, J. H. Bardarson, and M. Heyl, Sharp entanglement thresholds in the logarithmic negativity of disjoint blocks in the transverse-field Ising chain, *New J. Phys.* **20**, 083032 (2018).
- [73] N. Klco and M. J. Savage, Systematically localizable operators for quantum simulations of quantum field theories, *Phys. Rev. A* **102**, 012619 (2020).
- [74] G. Di Giulio and E. Tonni, On entanglement Hamiltonians of an interval in massless harmonic chains, *J. Stat. Mech.* (2020) 033102.
- [75] G. Giedke, B. Kraus, M. Lewenstein, and J. I. Cirac, Entanglement criteria for all bipartite Gaussian states, *Phys. Rev. Lett.* **87**, 167904 (2001).
- [76] A. Retzker, J. I. Cirac, and B. Reznik, Detecting vacuum entanglement in a linear ion trap, *Phys. Rev. Lett.* **94**, 050504 (2005).
- [77] S. P. Jordan, K. S. M. Lee, and J. Preskill, Quantum computation of scattering in scalar quantum field theories, *Quantum Inf. Comput.* **14**, 1014 (2014).
- [78] S. P. Jordan, K. S. M. Lee, and J. Preskill, Quantum algorithms for quantum field theories, *Science* **336**, 1130 (2012).
- [79] J. Kempe, A. Kitaev, and O. Regev, The complexity of the local Hamiltonian problem, *SIAM J. Comput.* **35**, 1070 (2006).
- [80] R. Oliveira and B. M. Terhal, The complexity of quantum spin systems on a two-dimensional square lattice, *Quantum Inf. Comput.* **8**, 0900 (2008).
- [81] M. H. Freedman and M. B. Hastings, Quantum systems on non-k-hyperfinite complexes: A generalization of classical statistical mechanics on expander graphs, *Quantum Inf. Comput.* **14**, 144 (2014).
- [82] A. Anshu, N. P. Breuckmann, and C. Nirkhe, NLTS Hamiltonians from good quantum codes, in *Proceedings of the 55th Annual ACM Symposium on Theory of Computing* (Associ-

- ation for Computing Machinery, New York, NY, 2003), pp. 1090–1096.
- [83] A. Kitaev and W. A. Webb, Wavefunction preparation and resampling using a quantum computer, [arXiv:0801.0342](https://arxiv.org/abs/0801.0342).
- [84] D. B. Kaplan, N. Klco, and A. Roggero, Ground states via spectral combing on a quantum computer, [arXiv:1709.08250](https://arxiv.org/abs/1709.08250).
- [85] A. Hamed Moosavian and S. Jordan, Faster quantum algorithm to simulate fermionic quantum field theory, *Phys. Rev. A* **98**, 012332 (2018).
- [86] D. Lee, J. Bonitati, G. Given, C. Hicks, N. Li, B.-N. Lu, A. Rai, A. Sarkar, and J. Watkins, Projected cooling algorithm for quantum computation, *Phys. Lett. B* **807**, 135536 (2020).
- [87] A. H. Moosavian, J. R. Garrison, and S. P. Jordan, Site-by-site quantum state preparation algorithm for preparing vacua of fermionic lattice field theories, [arXiv:1911.03505](https://arxiv.org/abs/1911.03505).
- [88] K. Choi, D. Lee, J. Bonitati, Z. Qian, and J. Watkins, Rodeo algorithm for quantum computing, *Phys. Rev. Lett.* **127**, 040505 (2021).
- [89] A. J. Buser, T. Bhattacharya, L. Cincio, and R. Gupta, State preparation and measurement in a quantum simulation of the $O(3)$ sigma model, *Phys. Rev. D* **102**, 114514 (2020).
- [90] N. Klco and M. J. Savage, Fixed-point quantum circuits for quantum field theories, *Phys. Rev. A* **102**, 052422 (2020).
- [91] L. Lin and Y. Tong, Near-optimal ground state preparation, *Quantum* **4**, 372 (2020).
- [92] P. Deliyannis, M. Freytsis, B. Nachman, and C. W. Bauer, Practical considerations for the preparation of multivariate Gaussian states on quantum computers, [arXiv:2109.10918](https://arxiv.org/abs/2109.10918).
- [93] A. N. Ciavarella and I. A. Chernyshev, Preparation of the $SU(3)$ lattice Yang-Mills vacuum with variational quantum methods, *Phys. Rev. D* **105**, 074504 (2022).
- [94] L. Funcke, T. Hartung, K. Jansen, S. Kühn, M. Schneider, P. Stornati, and X. Wang, Towards quantum simulations in particle physics and beyond on noisy intermediate-scale quantum devices, *Philos. Trans. R. Soc. A* **380**, 20210062 (2021).
- [95] M. Bagherimehrab, Y. R. Sanders, D. W. Berry, G. K. Brennen, and B. C. Sanders, Nearly optimal quantum algorithm for generating the ground state of a free quantum field theory, *PRX Quantum* **3**, 020364 (2022).
- [96] I. Stetcu, A. Baroni, and J. Carlson, Projection algorithm for state preparation on quantum computers, *Phys. Rev. C* **108**, L031306 (2023).
- [97] R. C. Farrell, M. Illa, A. N. Ciavarella, and M. J. Savage, Scalable circuits for preparing ground states on digital quantum computers: The Schwinger model vacuum on 100 qubits, *PRX Quantum* **5**, 020315 (2024).
- [98] T. D. Cohen and H. Oh, Efficient vacuum state preparation for quantum simulation of strongly interacting local quantum field theories, *Phys. Rev. A* **109**, L020402 (2024).
- [99] E. H. Lieb and D. W. Robinson, The finite group velocity of quantum spin systems, *Commun. Math. Phys.* **28**, 251 (1972).
- [100] B. Nachtergaele, Y. Ogata, and R. Sims, Propagation of correlations in quantum lattice systems, *J. Stat. Phys.* **124**, 1 (2006).
- [101] A. Uhlmann, The “transition probability” in the state space of a $*$ -algebra, *Rep. Math. Phys.* **9**, 273 (1976).
- [102] R. Jozsa, Fidelity for mixed quantum states, *J. Mod. Opt.* **41**, 2315 (1994).
- [103] C. A. Fuchs, Distinguishability and accessible information in quantum theory, Ph.D. thesis, New Mexico University, 1995.
- [104] C. Helstrom, Minimum mean-squared error of estimates in quantum statistics, *Phys. Lett. A* **25**, 101 (1967).
- [105] D. Bures, An extension of kakutani’s theorem on infinite product measures to the tensor product of semifinite w^* -algebras, *Trans. Am. Math. Soc.* **135**, 199 (1969).
- [106] L. Banchi, S. L. Braunstein, and S. Pirandola, Quantum fidelity for arbitrary Gaussian states, *Phys. Rev. Lett.* **115**, 260501 (2015).
- [107] D. J. Heinzen and D. J. Wineland, Quantum-limited cooling and detection of radio-frequency oscillations by laser-cooled ions, *Phys. Rev. A* **42**, 2977 (1990).
- [108] J. I. Cirac, A. S. Parkins, R. Blatt, and P. Zoller, “Dark” squeezed states of the motion of a trapped ion, *Phys. Rev. Lett.* **70**, 556 (1993).
- [109] D. M. Meekhof, C. Monroe, B. E. King, W. M. Itano, and D. J. Wineland, Generation of nonclassical motional states of a trapped atom, *Phys. Rev. Lett.* **76**, 1796 (1996).
- [110] J. Alonso, F. M. Leupold, B. C. Keitch, and J. P. Home, Quantum control of the motional states of trapped ions through fast switching of trapping potentials, *New J. Phys.* **15**, 023001 (2013).
- [111] D. Kienzler, H. Y. Lo, B. Keitch, L. de Clercq, F. Leupold, F. Lindenefelder, M. Marinelli, V. Negnevitsky, and J. P. Home, Quantum harmonic oscillator state synthesis by reservoir engineering, *Science* **347**, 53 (2015).
- [112] D. Kienzler, C. Flühmann, V. Negnevitsky, H. Y. Lo, M. Marinelli, D. Nadlinger, and J. P. Home, Observation of quantum interference between separated mechanical oscillator wave packets, *Phys. Rev. Lett.* **116**, 140402 (2016).
- [113] S. C. Burd, R. Srinivas, J. J. Bollinger, A. C. Wilson, D. J. Wineland, D. Leibfried, D. H. Slichter, and D. T. C. Allcock, Quantum amplification of mechanical oscillator motion, *Science* **364**, 1163 (2019).
- [114] R. T. Sutherland, S. C. Burd, D. H. Slichter, S. B. Libby, and D. Leibfried, Motional squeezing for trapped ion transport and separation, *Phys. Rev. Lett.* **127**, 083201 (2021).
- [115] P. Gokhale, J. M. Baker, C. Duckering, N. C. Brown, K. R. Brown, and F. T. Chong, Asymptotic improvements to quantum circuits via qutrits, in *Proceedings of the 46th International Symposium on Computer Architecture* (Association for Computing Machinery, New York, NY, 2019), pp. 554–566.
- [116] P. J. Low, B. M. White, A. A. Cox, M. L. Day, and C. Senko, Practical trapped-ion protocols for universal qudit-based quantum computing, *Phys. Rev. Res.* **2**, 033128 (2020).
- [117] M. S. Blok, V. V. Ramasesh, T. Schuster, K. O’Brien, J. M. Kreikebaum, D. Dahlen, A. Morvan, B. Yoshida, N. Y. Yao, and I. Siddiqi, Quantum information scrambling on a superconducting qutrit processor, *Phys. Rev. X* **11**, 021010 (2021).
- [118] A. Ciavarella, N. Klco, and M. J. Savage, Trailhead for quantum simulation of $SU(3)$ Yang-Mills lattice gauge theory in the local multiplet basis, *Phys. Rev. D* **103**, 094501 (2021).
- [119] D. M. Kurkcuoglu, M. S. Alam, A. C. Y. Li, A. Macridin, and G. N. Perdue, Quantum simulation of ϕ^4 theories in qudit systems, [arXiv:2108.13357](https://arxiv.org/abs/2108.13357).
- [120] Y. Chi *et al.*, A programmable qudit-based quantum processor, *Nat. Commun.* **13**, 1166 (2022).
- [121] E. Gustafson, Noise improvements in quantum simulations of sQED using qutrits, [arXiv:2201.04546](https://arxiv.org/abs/2201.04546).

- [122] N. Goss, A. Morvan, B. Marinelli, B. K. Mitchell, L. B. Nguyen, R. K. Naik, L. Chen, C. Jünger, J. M. Kreikebaum, D. I. Santiago, J. J. Wallman, and I. Siddiqi, High-fidelity qutrit entangling gates for superconducting circuits, *Nat. Commun.* **13**, 7481 (2022).
- [123] D. González-Cuadra, T. V. Zache, J. Carrasco, B. Kraus, and P. Zoller, Hardware efficient quantum simulation of non-Abelian gauge theories with qudits on Rydberg platforms, *Phys. Rev. Lett.* **129**, 160501 (2022).
- [124] T. V. Zache, D. González-Cuadra, and P. Zoller, Fermion-qudit quantum processors for simulating lattice gauge theories with matter, *Quantum* **7**, 1140 (2023).
- [125] P. P. Popov, M. Meth, M. Lewenstein, P. Hauke, M. Ringbauer, E. Zohar, and V. Kasper, Variational quantum simulation of U(1) lattice gauge theories with qudit systems, *Phys. Rev. Res.* **6**, 013202 (2024).
- [126] P. J. Low, B. White, and C. Senko, Control and readout of a 13-level trapped ion qudit, [arXiv:2306.03340](https://arxiv.org/abs/2306.03340).
- [127] M. Meth, J. F. Haase, J. Zhang, C. Edmunds, L. Postler, A. Steiner, A. J. Jena, L. Dellantonio, R. Blatt, P. Zoller, T. Monz, P. Schindler, C. Muschik, and M. Ringbauer, Simulating 2D lattice gauge theories on a qudit quantum computer [arXiv:2310.12110](https://arxiv.org/abs/2310.12110).
- [128] W. Son, M. S. Kim, J. Lee, and D. Ahn, Entanglement transfer from continuous variables to qubits, *J. Mod. Opt.* **49**, 1739 (2002).
- [129] B. Kraus and J. I. Cirac, Discrete entanglement distribution with squeezed light, *Phys. Rev. Lett.* **92**, 013602 (2004).
- [130] M. Paternostro, W. Son, M. S. Kim, G. Falci, and G. M. Palma, Dynamical entanglement transfer for quantum-information networks, *Phys. Rev. A* **70**, 022320 (2004).
- [131] A. Serafini, M. Paternostro, M. S. Kim, and S. Bose, Enhanced dynamical entanglement transfer with multiple qubits, *Phys. Rev. A* **73**, 022312 (2006).
- [132] F. Casagrande, A. Lulli, and M. G. A. Paris, Improving the entanglement transfer from continuous-variable systems to localized qubits using non-Gaussian states, *Phys. Rev. A* **75**, 032336 (2007).
- [133] T. Byrnes and Y. Yamamoto, Simulating lattice gauge theories on a quantum computer, *Phys. Rev. A* **73**, 022328 (2006).
- [134] E. Zohar, J. I. Cirac, and B. Reznik, Quantum simulations of gauge theories with ultracold atoms: Local gauge invariance from angular momentum conservation, *Phys. Rev. A* **88**, 023617 (2013).
- [135] E. A. Martinez, C. A. Muschik, P. Schindler, D. Nigg, A. Erhard, M. Heyl, P. Hauke, M. Dalmonte, T. Monz, P. Zoller *et al.*, Real-time dynamics of lattice gauge theories with a few-qubit quantum computer, *Nature (London)* **534**, 516 (2016).
- [136] I. Raychowdhury and J. R. Stryker, Solving Gauss's law on digital quantum computers with loop-string-hadron digitization, *Phys. Rev. Res.* **2**, 033039 (2020).
- [137] N. Klco and M. J. Savage, Digitization of scalar fields for quantum computing, *Phys. Rev. A* **99**, 052335 (2019).
- [138] A. Alexandru, P. F. Bedaque, S. Harmalkar, H. Lamm, S. Lawrence, and N. C. Warrington (NuQS Collaboration), Gluon field digitization for quantum computers, *Phys. Rev. D* **100**, 114501 (2019).
- [139] N. Klco, M. J. Savage, and J. R. Stryker, SU(2) non-Abelian gauge field theory in one dimension on digital quantum computers, *Phys. Rev. D* **101**, 074512 (2020).
- [140] M. Kreshchuk, W. M. Kirby, G. Goldstein, H. Beauchemin, and P. J. Love, Quantum simulation of quantum field theory in the light-front formulation, *Phys. Rev. A* **105**, 032418 (2022).
- [141] Z. Davoudi, I. Raychowdhury, and A. Shaw, Search for efficient formulations for Hamiltonian simulation of non-Abelian lattice gauge theories, *Phys. Rev. D* **104**, 074505 (2021).
- [142] J. F. Haase, L. Dellantonio, A. Celi, D. Paulson, A. Kan, K. Jansen, and C. A. Muschik, A resource efficient approach for quantum and classical simulations of gauge theories in particle physics, *Quantum* **5**, 393 (2021).
- [143] C. W. Bauer and D. M. Grabowska, Efficient representation for simulating U(1) gauge theories on digital quantum computers at all values of the coupling, *Phys. Rev. D* **107**, L031503 (2023).
- [144] U.-J. Wiese, From quantum link models to D-theory: A resource efficient framework for the quantum simulation and computation of gauge theories, *Philos. Trans. R. Soc. A* **380**, 20210068 (2021).
- [145] M. Aidelsburger, L. Barbiero, A. Bermudez, T. Chanda, A. Dauphin, D. González-Cuadra, P. R. Grzybowski, S. Hands, F. Jendrzejewski, J. Jünemann *et al.*, Cold atoms meet lattice gauge theory, *Philos. Trans. R. Soc. A* **380**, 20210064 (2021).
- [146] G. Pardo, T. Greenberg, A. Fortinsky, N. Katz, and E. Zohar, Resource-efficient quantum simulation of lattice gauge theories in arbitrary dimensions: Solving for Gauss's law and fermion elimination, *Phys. Rev. Res.* **5**, 023077 (2023).
- [147] S. V. Kadam, I. Raychowdhury, and J. R. Stryker, Loop-string-hadron formulation of an SU(3) gauge theory with dynamical quarks, *Phys. Rev. D* **107**, 094513 (2023).
- [148] C. W. Bauer, Z. Davoudi, N. Klco, and M. J. Savage, Quantum simulation of fundamental particles and forces, *Nat. Rev. Phys.* **5**, 420 (2023).
- [149] I. D'Andrea, C. W. Bauer, D. M. Grabowska, and M. Freytsis, A new basis for Hamiltonian SU(2) simulations, *Phys. Rev. D*, **109**, 074501 (2024).
- [150] L. Funcke, T. Hartung, K. Jansen, and S. Kühn, Review on quantum computing for lattice field theory, *Proc. Sci.* **430**, 228 (2023).
- [151] R. Gilmore, Baker-Campbell-Hausdorff formulas, *J. Math. Phys.* **15**, 2090 (1974).
- [152] M. A. M. Santiago, Baker-Campbell-Hausdorff formulae and spherical and hyperbolic rotations, *J. Phys. A* **9**, 897 (1976).
- [153] C. S. Hamilton, R. Kruse, L. Sansoni, S. Barkhofen, C. Silberhorn, and I. Jex, Gaussian boson sampling, *Phys. Rev. Lett.* **119**, 170501 (2017).
- [154] R. Kruse, C. S. Hamilton, L. Sansoni, S. Barkhofen, C. Silberhorn, and I. Jex, Detailed study of Gaussian boson sampling, *Phys. Rev. A* **100**, 032326 (2019).
- [155] N. Quesada, L. G. Helt, J. Izaac, J. M. Arrazola, R. Shahrokhshahi, C. R. Myers, and K. K. Sabapathy, Simulating realistic non-Gaussian state preparation, *Phys. Rev. A* **100**, 022341 (2019).
- [156] B. Arvind, Dutta, N. Mukunda, and R. Simon, The real symplectic groups in quantum mechanics and optics, *Pramana* **45**, 471 (1995).
- [157] S. L. Braunstein, Squeezing as an irreducible resource, *Phys. Rev. A* **71**, 055801 (2005).